POLITECNICO
MILANO 1863

School of Industrial and Information Engineering
Department of Aerospace Science and Technology

Master of Science in Space Engineering

Continuous-thrust collision avoidance manoeuvres optimization

Advisor: Dr. Pierluigi Di Lizia
Co-Advisor: Dr. Roberto Armellin

M.Sc. Dissertation of:
Giuseppina SALEMME
Matr. 875265

Academic Year 2018-2019

Alla mia famiglia,
Grazie.

"There was a smell of Time in the air tonight. He smiled and turned the fancy in his mind. There was a thought. What did time smell like? Like dust and clocks and people. And if you wondered what Time sounded like it sounded like water running in a dark cave and voices crying and dirt dropping down upon hollow box lids, and rain. And, going further, what did Time look like? Time look like snow dropping silently into a black room or it looked like a silent film in an ancient theater, 100 billion faces falling like those New Year balloons, down and down into nothing. That was how Time smelled and looked and sounded. And tonight-Tomas shoved a hand into the wind outside the truck-tonight you could almost taste time."

— Ray Bradbury, The Martian chronicles

ABSTRACT

In the last few decades, space debris have become one of the most important hazards for space activities; preventing their formation is the best mitigation option, and avoiding an impact can be of fundamental importance for a mission's success. This study proposes four methods to design a continuous-thrust Collision Avoidance Manoeuvre (CAM), which have been developed in the perspective of finding a fast and reliable approach, suitable for on-board implementation. The objective function to be minimized is the collision probability (Pc) at the nominal time of closest approach. The first approach consists in the conversion from an analytical fuel-optimal impulsive manoeuvre to a finite-burn arc through an indirect optimal control model. In the second approach, a new formulation of the problem is proposed, where the collision probability is considered as a terminal constraint in the minimum-Fuel and minimum-Energy Optimal Control Problem (FOP/EOP). The mathematical formulation yields a Two Boundary Value Problem, whose minimum-fuel discontinuous solution is achieved through a continuation method, and the shooting method is adopted for the resolution of the minimum-energy formulation. Both of these approaches require time consuming fully numerical iterative cycles. The last two methods are based on the linearisation of EOP, and consist in an analytical and semi-analytical approach. In the analytical approach the direction of maximum change of Pc is exploited, in order to obtain the maximum decrease of Pc with the least deviation from the nominal trajectory. In the semi-analytical approach, the boundary conditions of the TPBVP associated to the minimum-energy problem are exploited, leading to a relation between the terminal cost in the cost function and the final spacecraft position. All these approaches are compared via a numerical test case set in the two-body dynamical framework, assuming circular Keplerian orbits.

SOMMARIO

Negli ultimi decenni, i detriti spaziali sono diventati uno dei maggiori pericoli per le attività spaziali; prevenirne la formazione è la migliore strategia di mitigazione, ed evitare un impatto può essere di importanza vitale per il successo di una missione. Questo studio propone quattro metodi per progettare una manovra per evitare la collisione (CAM) a spinta finita, sviluppati nell'ottica di trovare un approccio veloce e robusto, adatto all'implementazione a bordo. L'obiettivo è minimizzare la probabilità di collisione (Pc) all'istante nominale di distanza minima. Il primo metodo consiste nella conversione di una manovra ottima impulsiva in un arco finito di spinta (FBC) attraverso un modello di controllo ottimo indiretto. Nel secondo approccio è proposta una nuova formulazione del problema, dove Pc è inserita come costo finale in un problema di controllo ottimo (OCP) nelle formulazioni a minima energia e minimo propellente. Tramite l'uso dei moltiplicatori di Lagrange e il calcolo variazionale, il problema diventa trovare i valori iniziali dei moltiplicatori. La soluzione a minimo propellente ha un profilo discontinuo e, di conseguenza, per evitare problemi numerici, è adottato un metodo di continuazione sulla spinta. La formulazione a minima energia è risolta tramite l'utilizzo dello shooting method. I precedenti due metodi sono interamente numerici e di difficile risoluzione a causa di possibili problemi numerici. Gli ultimi due metodi sono basati sulla linearizzazione dell' OCP formulato nella versione a minima energia (EOP), e consistono in un approccio analitico ed in uno semi-analitico. Nell'approccio analitico è sfruttata la direzione dove Pc varia più velocemente, in modo tale da ottenere la massima diminuzione di Pc con la minima deviazione dalla traiettoria nominale. Nell'approccio semi-analitico vengono sfruttate le condizioni finali sui moltiplicatori ricavate dall'applicazione dell' OCP, le quali permettono di ottenere una relazione tra il costo finale nella funzione obiettivo e la probabilità risultante. Tutti i precedenti approcci sono comparati tra loro attraverso un caso reale nel contesto del problema dei due corpi, considerando orbite Kepleriane circolari.

ESTRATTO DELLA TESI DI LAUREA

Questo lavoro si focalizza sull'ottimizzazione della manovre per evitare la collisione (CAM). Negli ultimi decenni, i detriti spaziali sono diventati uno dei maggiori pericoli per le attività spaziali, e prevenirne la formazione è la migliore strategia di mitigazione. Queste manovre sono programmate quando un determinato limite sulla probabilità di collisione (P_c) o sulla minima distanza tra l'oggetto manovrabile e l'oggetto seciondario, è superato. Dato l'alto numero di avvisi su possibli collisioni e la limitata disponibilità di carburante, le CAM sono progettate per essere il più efficienti possibili in termine di carburante, così come rispettose dei requisiti di missione.

Al momento le manovre sono programmate a terra, e non sono disponibili sistemi autonomi di progettazioni implementabili a bordo. In questa tesi vengono investigate quattro diverse soluzioni al problema della minimizzazione della probabilità di collisione, sviluppate con lo scopo di trovare un metodo veloce ed robusto, adatto all'implementazione a bordo.

CAPITOLO 1

Nel primo capitolo viene introdotto il contesto nel quale sia articola questa dissertazione. Nella prima parte è brevemente spiegato il problema dei detriti spaziali, e come viene gestito al momento. Nella seconda parte sono illustrate le varie opzioni al momento disponibili per la progettazione di una CAM.

CAPITOLO 2

Nel secondo capitolo è illustrato il background matematico necessario per comprendere gli argomenti trattati nei capitoli seguenti. Dopo una breve intruduzione sul problema dei due corpi, e' dettagliatamente spiegato il modello usato per il calcolo della probabilità di collisione, mettendo in evidenza le ipotesi fatte. In seguito è rivista la teoria relativa al problema di controllo ottimo (OCP), nelle formulazioni a minimo consumo di propellente e minima energia. In fine è spiegato il processo usato da per la progettazione di una manovra ottima in caso di spinta impulsiva.

CAPITOLO 3

Nel terzo capitolo sono illustrati i diversi approcci sviluppati in questa tesi per minimizzare P_c. Il primo metodo consiste nella conversione di una manovra ottima impulsiva in un arco finito di spinta (FBC). La conversione si basa sul problema di controllo ottimo nella formulazione a minimo consumo di propellente. Inserendo le equazioni del moto nella funzione di costo e successivamente tramite l'uso dei moltiplicatori di Lagrange e il calcolo variazionale, il problema diventa trovare i valori iniziali dei moltiplicatori. La soluzione ottima ha un profilo discontinuo e, di conseguenza, per evitare problemi numerici, è adottato un metodo di continu-

azione sulla spinta. La spinta viene approssimata da un profilo esponenziale, e tramite continuazione su un parametro p, il profilo bang-bang viene iterativamente approssimato, al fine di recuperare la soluzione discontinua.

Il secondo metodo consiste nell'appilcazione del problema di controllo ottimo nella formulazione a minimo propellente (FOP) e minima energia (EOP), inserendo P_c nella funzione di costo da minimizzare sotto forma di costo finale. Nel FOP è adottato nuovamente il metodo di continuazione già usato per il primo metodo. Allo scopo di risolvere FBC e FOP, è usata la funzione MATLAB bvp4c, la quale necessita di soluzioni di primo tentativo. Allo scopo di trovare soluzioni di primo tentativo appropriate, l' Adjoint Control Transformation sviluppata in [23] è implementata. Il problema a minima energia, a differenza del FOP, ha soluzione di spinta continua. Conseguentemente, è possibile utilizzare lo shooting method per la sua risoluzione, dove la traiettoria è propagata in avanti e tramite iterazioni di Newton i moltiplicatori iniziali vengono variati finchè le condizioni finali sullo stato e moltiplicatori non sono rispettate. In entrambe le formulazioni, la funzione di costo è modificata tramite l'inserimento di pesi su P_c, in modo da variare l'importanza relativa assegnata alla probabilità e al consumo di massa/energia, ed ottenere profili diversi di P_c al momento previsto di collisione.

I precedenti due metodi sono interamente numerici e di difficile risoluzione a causa di possibili problemi numerici. Conseguentemente, non sono adatti alla implementazione a bordo. Il terzo e quarto metodo partono dalla linearizzazione dell'EOP, il primo risultante in un approccio analitico, il secondo in un approccio semi-analitico.

Nel terzo approccio, tramite un semplice problema agli autovalori, è trovata la direzione di massima variazione di P_c al tempo di prevista collisione. Spostanto la posizione finale del satellite lungo questa direzione, è possibile ottenere la massima viariazione di P_c con la minima deviazione dalla traiettoria nominale. In tal modo, il problema presenta stati iniziali e finali fissati. Tramite la State Transition Matrix (STM) risultante dalla linearizzazione dell'EOP, i moltiplicatori iniziali sono calcolati.

Nell'ultimo approccio, vengono sfruttate le condizioni finali sui moltiplicatori ricavate dall'applicazione dell' OCP. Lo scopo è quello di trovare una relazione diretta tra il peso inserito nella funzione di costo e la probabilità risultante. Tramite manipolazione della STM, è trovata una relazione non-lineare tra posizione finale e peso. Essendo P_c dipendente solo dalla posizione, tramite risoluzione dell'equazione è possibile ottenere la relazione desiderata.

CAPITOLO 4

Nel quarto capitolo sono mostrati i risultati numerici dei vari metodi. Il caso reale esaminato è quello della collisione tra satelliti, avvenuta il 10 febbraio 2009, che ha coinvolto il satellite operativo Iridium 33 e il detrito Cosmos 2251. I vari approcci sono confrontati in termini di massa, velocità di calcolo, e convergenza.

CAPITOLO 5

Nel quinto ed ultimo capitolo, sono tratte le conclusioni sul lavoro svolto, e vengono illustrati i possibili sviluppi futuri.

ACKNOWLEDGEMENTS

I would like to express my gratitude to my advisors, Dr. Pierluigi Di Lizia and Dr. Roberto Armellin. I truly appreciate the time you dedicated to me and the enthusiasm you showed. I could not have hoped for better mentors.

My deepest gratitude goes to my family. Mother, Father and Brother, without your support none of this would have been possible.

I am grateful to all the persons that crossed my path and made these years better than my higher expectations.
Giulio, you are the milestone, meeting you was one of the luckiest moments of my life; Marco, thank you for roaming the roads of Milano with me and Giulio in our first nights; Mecca, I relied on you more than you know: for the usual days and the special days, for the brave nights and the patio nights, Giulio, Basa, Gian, Fra, Dau, Fabio, Ivan, Dr2, Giovanni, Antonio, Emilio, Sofia, thank you; Federico, thank you for making me finish my Bachelor laughing. To all the amazing guys I met at SSC: Corinna, Gianluca, Silvia, Laura, Marcello, Alessandro, Salvatore, Andrea, David, Donato, Emilia, Harry, Lara, Lotfi, Sadra, Thomas, Pasquale, Antonio, Magda, Asma, Zack, thank you for making my experience worth remember, I am incredibly glad I had the opportunity to meet you. Ale, Simo, Fil, a toast to us, thank you for being my prodigious team; Fra, thank you, because you showed me that adventure smells of cinnamon and distant fires.

CONTENTS

LIST OF FIGURES

LIST OF TABLES

NOMENCLATURE

C	covariance matrix (km²).
H	Hamiltonian.
I_s	specific impulse (s).
J	cost function.
L	Lagrangian.
P_c	collision probability.
R_b	rotation matrix from ECI to b-plane.
S_f	switching function.
T	thrust (N).
W	weight.
$\Delta\theta$	angular distance from the collision (number of orbits).
Ω	right ascension of the ascending node (deg).
Φ	state transition matrix (or terminal cost).
$\delta(\cdot)$	variation of $(\cdot)$ with respect to the nominal trajectory.
ϵ_{AM}	position on $\mathbf{d}_{max}$.
η_c	finite-burn conversion efficiency.
γ	out-of-plane thrust angle (deg).
$\boldsymbol{\gamma}$	thrust direction.
$\boldsymbol{\lambda}$	costate vector.
$\mathbf{a}_c$	control acceleration (km/s²).
$\mathbf{d}_{max}$	direction of maximum change of P_c.
$\mathbf{r}$	position of the primary object (km).
$\mathbf{r}_b$	position of the primary object on b-plane (km).
$\mathbf{r}_c$	position of the primary object at the time of closest approach (km).
μ	Earth gravitational constant (km³/s²).
ω	argument of periapsis (deg).

ρ correlation coefficient.

σ standard deviation (or in-plane thrust angle) (km or deg).

θ true anomaly (deg).

a semi-major axis (km).

c_e effective velocity (km/s).

d miss distance (km).

e eccentricity.

i inclination (deg).

m mass (kg).

p continuation parameter.

r_a combined cross-sectional radius (km).

tc time to collision (s).

u thrust ratio.

v velocity (km/s).

ABBREVIATIONS

ACT	Adjoint Control Transformation.
AM	Analytical Method.
BC	Boundary Condition.
CAM	Collision Avoidance Manoeuvre.
CSM	Conjunction Summary Message.
CT	Computational Time.
ECI	Earth-Centered Inertial reference frame.
EOP	Energy-Optimal Problem.
FBC	Finite-Burn Conversion.
FOP	Fuel-Optimal Problem.
GEO	Geostationary Orbit.
IC	Initial Condition.
ISS	International Space Station.
JSpOC	Joint Space Operations Center.
LEO	Low Earth Orbit.
OCP	Optimal Control Problem.
PDF	Probability Density Function.
SAM	Semi-Analytical Method.
SSA	Space Situational Awareness Programme.
STM	State Transition Matrix.
TLE	Two Line Element set.
TOF	Time Of Flight.
TPBVP	Two Point Boundary Value Problem.
USSTRATCOM	U.S. Strategic Command.

1 INTRODUCTION

1.1 SPACE DEBRIS

Space debris are defined as human-generated, non-functional objects in Earth orbit or re-entering the atmosphere, and since space activity begun, almost 60 years ago, space debris accumulated in near-Earth space and now they represent a real threat to space activities. Statistical models estimate that more than 34000 objects bigger than 10cm, and hundreds of millions of objects which size range from 1mm to 1cm, are in orbit around the Earth [4].

The main sources of space debris include spent upper stages, fragments from explosions of satellites and rocket bodies, caused by the lost of mechanical integrity due to the space environment which leads to fuel self ignition, and antisatellite test (the Chinese FengYun-1C engagement in January 2007 alone increase the trackable space object population by 25%) [2]. Other important sources of debris are solid rocket motors, which firings release aluminium oxide in the form of particles even centimetres big, and ultraviolet radiation, which erodes surfaces causing the realising of paint droplets which sizes can be up to millimetres big.

Space debris are a navigation hazard to all operational satellites; in the event of a collision, due to the very high relative velocities, even few millimetres size debris can critically damage a satellite, ending the mission. Collision within bigger objects can be a disastrous event, leading to the formation of thousands more objects, as happened in 2009, when the accidental in-orbit collision between two satellites took place: the Iridium-33/Kosmos2251 collision produced more than 2300 trackable fragments.

Debris distribution in space is not uniform, it is higher in the most used space regions: that's why most space debris are concentrated in LEO and in GEO orbits, respectively where Earth observation satellites and telecommunications satellites work. For example, in 2016 the Russian Briz-M rocket underwent an in-orbit break-up, last of other three significant events involving Britz-M upper stages between 2006 and 2012, which altogether created thousands of debris whose orbits intersect the International Space Station (ISS) orbit and satellites in GEO. Assuming break-ups will continue at the same rates of the last decades, the number of debris will increase, and with it, the probability of catastrophic collisions. Prevention through post-mission disposal guidelines and active strategies to remove debris are crucial to keep some orbit regions accessible, since collisions create more debris creating a runaway chain reaction, known as the Kessler Syndrome: once the amount of debris in a particular orbit reaches critical mass, collision cascading begins even if no more objects are injected into orbit. At that point, the collision risk becomes unacceptable, and the orbit is no longer available[2].

Avoiding the collisions in the first place is the best mitigation strategy, and here's when collision avoidance manoeuvres come into play.

1.2 COLLISION AVOIDANCE MANOEUVRES (CAMS)

A collision avoidance manoeuvre is performed when, at the time of closest approach, a threshold on the miss distance, or on the collision probability, is exceeded: In the ISS case, for example, a manoeuvre is considered if the miss distance lies inside a box of $\pm 0.75 \times \pm 25 \times \pm 25$km in the UVW reference frame, while an usual probability threshold for LEO ESA's missions is $P > 10^{-4}$.

Until mid 2010, conjunctions were identified comparing mission orbits with the orbit informations of potential conjunction objects provided by USSTRATCOM in TLE format. Nowadays, conjunctions are detected thanks to Conjunction Summary Messages received by JSpOC.

A CSM is a message that contains information about a conjunction between a primary satellite and a secondary satellite; the CSM include also the time of closest approach, the miss distance, relative position and velocity in the Radial, In-track, Cross-track (UVW) reference frame, observation statistics, the satellite covariance matrices and the time of last acceptable observation. It is sent every time a pre-defined threshold on the miss distance or the collision probability is exceeded, and a satellite operator might receive up to 30 CSM per day. It is up to the satellite's operator, once the message is received, to decide if a manoeuvre is necessary or not. Detailed informations about CSM can be found in [8].

Being Europe mainly dependent on non-European sources of informations for what regards the capacity of watching for satellite's sources of danger like natural phenomena, NEO's and space debris, ESA is implementing the Space Situational Awareness (SSA) programme, a programme aimed to give Europe the necessary independence to acquire knowledge about the situation in space. SSA programme focuses on Space Weather, Near-Earth Objects, and Space Surveillance and Tracking. Providing independent data and informations, the SSA programme also strength the reliability and availability of space-based applications. An overview of the programme can be found in [11].

Because of the high number of warnings and of the limited fuel availability, collision avoidance manoeuvres are planned to be the most efficient as possible in terms of propellant, as well as most compliant as possible with mission requirements: because of the increasing number of objects in orbit, efficient manoeuvres are essential to extend a mission's life. As explained in [13], planning, implementation and execution of collision avoidance manoeuvres takes several hours: the current ESA's routine, once a CSM is received, includes tracking data, updating ephemerides, covariances and conjunction geometries and re-estimating the collision risk. If the risk is still considered high enough to require a collision avoidance manoeuvre, the manoeuvre has to be planned, and even if only 2% of the conjunctions are predicted less than 24 hours in advance, the need of fast responses can only increase, as the space debris situation gets worse.

Nowadays manoeuvres are planned on-ground, and no on-board autonomous collision avoidance manoeuvres planning tools are available: because of the huge amount of data to process as the number of warnings increases, it is desirable to automate the process of screening, manoeuvre planning and execution.

1.3 STATE OF THE ART

Nowadays, CAMs are planned on-ground, with the support of specific tools. If the pre-defined threshold on the probability or on the miss distance is exceeded, a manoeuvre is designed by mission planners.

Regarding ESA, the Space Debris Office (SDO) is the department in charge of all the activities concerning space debris. The ARES tool [10] (within the DRAMA tool suite) is used in order to estimate a proper reaction threshold, through a trade-off between ignored risk and avoided risk. When a CSM is received, the CORAM software is used to compute the associated risk. If a manoeuvre is considered necessary, the CAMOS (Collision Avoidance Manoeuvre Optimization Software) tool of CORAM [14] is used to support manoeuvre planning and optimization. A full description of the SDO current collision avoidance service can bee found in [20]

The U.S. National Security Space Systems, through the support of the Aerospace Corporation, relies on the Collision Vision software [22]: in order to support mission planners, several manoeuvres are found through a search in the four-dimensional space composed by the manoeuvre time, velocity magnitude and the velocity direction angles.

Algorithms for the design of CAMs often employ direct optimization methods. In [3] a mixed-integer linear programming method is used to find fuel-optimal trajectories for spacecraft subjected to avoidance requirements. CAMOS exploits a method based on a parametric search. In [22] the dimension of the problem is reduced from three to one, decoupling thrust direction and thrust magnitude, and a method based on a gradient search is developed. In [24] a fuel-optimal manoeuvre is found through the implementation of a genetic algorithm. Multi-objective particle swarm optimizers are employed by [21] to design an optimal continuous-thrust CAM. Research on continuous-thrust optimization methods includes the semi-analytical method developed by [25] for rapid collision avoidance, based on the hypothesis that the optimal thrust is always radial. [18] developed an analytical solution to the problem of maximizing the miss distance through the use of generating functions, inserting the miss distance as penalty function in an optimal feedback control problem. The lack of iterative processes is counteracted by the sub-optimality of the solution and the empirical effort needed to tune the design parameters.

Optimal impulsive manoeuvres are studied in [27], where the problem is linearised and the minimum impulsive ΔV that respect a terminal position constraint is found through an eigenvalue problem, but the conclusions are not satisfactory if a precise control is required. Recently [6] developed an analytical and semi-analytical method to find the fuel-optimal impulsive collision avoidance manoeuvre in case of direct and non-direct impact.

1.4 MOTIVATIONS AND DISSERTATION OVERVIEW

In the last few decades, space debris have become one of the most important hazards for space activities; preventing their formation is the best mitigation option, and avoiding an impact can be of fundamental importance for a mission's success. This study proposes four methods to design a continuous-thrust CAM, where the

objective function to be minimized is the collision probability at the nominal time of closest approach. At the time of writing, little research regarding designing CAMs with small notification time is available, and no on-board autonomous CAM planning tool exists. Therefore, the approaches proposed in this work have been developed in the perspective of finding a fast and reliable approach, suitable for on-board implementation.

Chapter 2

The second chapter is devoted to review the mathematical background upon which the thesis is based. After a brief introduction on the two-body problem, the model used to compute the collision probability P_c is explained in detail, enlightening the adopted hypothesis. Afterwards, the theory relative to the Optimal Control Problem (OCP) is reviewed, with particular attention on the fuel/energy-minimum formulations (FOP/EOP). In the end, the optimal impulsive CAM designed by [6] is explained, and the theory behind the state transition matrix for time-varying systems is illustrated.

Chapter 3

In the third chapter the four approaches developed in order to minimize P_c are explained. The first method consists in the conversion of the impulsive CAM described in Chapter 2 to a finite-burn arc, trough an indirect optimization method, using the minimum-fuel formulation. The impulsive manoeuvre point is considered the middle point of the thrust arc, and the impulsive $\Delta\boldsymbol{v}$ is distributed over the arc bounded by the initial and final states, which are found by propagating backward and forward from the impulsive manoeuvre point over the pre-impulse and post-impulse trajectories. In the second approach the problem is stated as an OCP where the P_c computed with the Chan model is inserted in the cost function as terminal cost. Through the application of calculus of variations, FOP and EOP translate in the solution of a Two Point Boundary Value Problem (TPBVP), with the boundary conditions consisting in the initial state and final costate. The TPBVP associated to the FOP is solved with a collocation method, while EOP is solved through the adoption of the shooting method. The optimal control laws resulting from the fuel-optimal formulations (finite-burn conversion and FOP) require a continuation method on the thrust to achieve the optimal discontinuous solution. These processes are carried on a grid of initial manoeuvre points along the nominal orbit, and through the application of weights W in the cost function it is possible to tune the P_c for the same manoeuvre point: the weights change the ratio between the terminal and the path cost, so that a larger weight on P_c yields a lower collision probability at fuel's or energy's expense.

In the third approach EOP is linearised, and an analytical solution is obtained by computing and manipulating the State Transition Matrix (STM). The problem translates in a transfer between two fixed states: the direction of maximum change of P_c at the time of closest approach, $\mathbf{d}_{max}$, is found through a simple eigenvalue problem. The final position of the spacecraft $\mathbf{r}_f$ is set to be along this direction, in order to obtain the maximum change of P_c with the least deviation from the

nominal trajectory. Depending on the position of $\mathbf{r}_f$ along $\mathbf{d}_{max}$, different P_c are obtained.

The fourth approach starts from the linearisation of the EOP and exploits the boundary conditions of the TPBVP associated with the EOP to find a direct relation between the terminal cost in the cost function and $\mathbf{r}_f$. The application of different weights W to the terminal cost in the cost function affects the terminal boundary conditions of the costates. Through the STM, it is possible to obtain a set of nonlinear equations to find $\mathbf{r}_f$, function of W. Once $\mathbf{r}_f$ is obtained, P_c is immediately computed trough an analytical formula. By acting on the weight W, it is possible to tune P_c for the same manoeuvre point. Then, by means of the STM, the initial costate and the optimal control law associated to the desired P_c can be retrieved.

Chapter 4

In the fourth chapter the numerical results of the different methods are shown. The test case examined is the collision between the American communication satellite Iridium 33 and the derelict Russian communication satellite Cosmos 2251, happened on February 10^{TH}, 2009. The approaches are compared in terms of propellant mass, computational time and robustness.

Chapter 5

In the fifth and last chapter, the final considerations about this work are reported, as well as the possible future developments.

2

MATHEMATICAL MODEL

This chapter is devoted to review the mathematical background upon which the thesis is based. The first section concerns the adopted dynamical model. Then in Section 2.2 some basic concepts of probability theory are reviewed, in order to give to the reader the necessary tools for collision probability computation. In Section 2.3 the theory behind the formulation and resolution of an optimal control problem is examined, specifically in its energy/fuel formulations. Section 2.4 is dedicated to the overview of the method developed by [6] for the formulation of an impulsive optimal CAM, since its results are exploited multiple times in this dissertation. The last section is devoted to the theory behind the formulation of the state transition matrix for time-dependant linear systems, which is the foundation of the approaches in Section 3.5 and 3.6.

2.1 THE RESTRICTED TWO-BODY PROBLEM

In this section the dynamical model used to describe the motion of the primary satellite is illustrated. After a brief introduction of the n-body model, the equations of motion that describes the satellite's motion in the context of the 2-body dynamics are explained.

The more general n-body problem considers n point masses m_i, $i = 1, 2, \dots, n$ subjected only to their mutual gravitational attraction, in an inertial reference frame in the three dimensional space. Their motion is regulated by Newton universal gravitation law

$$m_i \ddot{\mathbf{r}}_i = \sum_{\substack{j=1 \\ j \neq i}}^{n} G \frac{m_i m_j}{r_{ji}^3} (\mathbf{r}_j - \mathbf{r}_i), \qquad i = 1, \dots n. \tag{1}$$

G is the universal gravitational constant and r_{ji} is the magnitude of the distance between two generic masses m_i, m_j.
A potential energy for the gravitational force can be defined, since it is a conservative force

$$U = \sum_{\substack{j=1 \\ j \neq i}}^{n} G \frac{m_i m_j}{r_{ji}}, \tag{2}$$

so that 1 can be rewritten in a more compact way, where ∇ is the gradient operator

$$m_i \ddot{\mathbf{r}}_i = \nabla U, \qquad i = 1, \dots, n.$$

This is a set of $6n$ first-order differential equations, and for $n > 2$ no closed form solution exists.
When the motion of a massless particle (a particle with a mass infinitesimally small with respect to the other bodies, for example a satellite) is studied, the problem is

called *restricted* n-body problem. For $n = 2$ the problem is completely solved and even if for Earth satellites it is not as representative of the actual dynamics as a 3-body model, it is often used for preliminary mission design stages. The equations of motion are

$$\ddot{\mathbf{r}} = -\frac{\mu}{r^3}\mathbf{r}\,, \tag{3}$$

where μ is the Earth gravitational constant. When also the control acceleration of the spacecraft is taken into account, $\mathbf{a_c} = T_{max}\frac{u}{m}\boldsymbol{\gamma}$, the set of first-order differential equations that describe the controlled dynamics is

$$\begin{cases} \dot{\mathbf{r}} = \boldsymbol{v}\,, \\ \dot{\boldsymbol{v}} = \mathbf{g}(\mathbf{r}) + T_{max}\frac{u}{m}\boldsymbol{\gamma}\,, \\ \dot{m} = -\frac{T_{max}u}{I_{sp}g_0}\,, \end{cases} \tag{4}$$

with

$$\mathbf{g}(\mathbf{r}) = \frac{\mu}{r^3}\mathbf{r}\,, \tag{5}$$

where T_{max} is the maximum thrust magnitude the propulsion system can provide, m is the spacecraft mass, u is the thrust ratio, $u \in [0, 1]$, I_{sp} is the thruster specific impulse, g_0 is the sea level gravity acceleration and $\boldsymbol{\gamma}$ is the thrust direction.

2.2 COLLISION PROBABILITY

In this section the basic concepts of probability theory needed to fully understand the topic of collision probability computation are reviewed. Next the b-plane, a reference frame that simplifies the understanding of the collision dynamics, is introduced, and the main hypothesis related to the computation of the collision probability are illustrated. Finally, the detailed method used to compute the collision probability is described.

2.2.1 *Review on probability theory*

The covariance function of a random process $\mathbf{x}(t)$ is defined as

$$\begin{aligned} C_{xx}(t_1, t_2) &= E[\Delta\mathbf{x}(t_1)\Delta\mathbf{x}^T(t_2)] \\ &= E[(\mathbf{x}(t_1) - \boldsymbol{\mu}_x(t_1))(\mathbf{x}(t_2) - \boldsymbol{\mu}_x(t_2))^T]\,, \end{aligned} \tag{6}$$

where $\boldsymbol{\mu}_x$ is the expected value, the average of all realizations of the process $\mathbf{x}(t)$, defined as

$$\boldsymbol{\mu}_x(t) = E[\mathbf{x}(t)] = \int_{-\infty}^{+\infty}\cdots\int_{-\infty}^{+\infty}\mathbf{x}f(\mathbf{x})d\mathbf{x}\,. \tag{7}$$

The function inside the integral is integrated as many times as the number of variables and $f(x)$ is the Probability Density Function (PDF) of the continuous random variable $\mathbf{x}$.

PDF is the derivative of the cumulative density function $F_{\mathbf{X}}(\mathbf{x})$, which represents the probability the variable $\mathbf{X}$ will fall into the interval $\mathbf{X} \in (-\infty, \mathbf{x}_i), i \in [1, n]$, n number of components of $\mathbf{X}$

$$F(\mathbf{x}) = \int_{-\infty}^{x_1} \cdots \int_{-\infty}^{x_n} f(\mathbf{u}) d\mathbf{u} \,. \tag{8}$$

We are interested in the error associated to the relative position of the primary spacecraft with respect to the secondary object. Defining the position of the primary spacecraft $\mathbf{r}_p$, and the position of the secondary object $\mathbf{r}_s$, the relative position is $\mathbf{r}_p - \mathbf{r}_s$, the mean relative position is $\bar{\mathbf{r}}_p - \bar{\mathbf{r}}_s$ and the covariance matrix is defined by

$$\begin{aligned} C &= E[((\mathbf{r}_p - \mathbf{r}_s) - (\bar{\mathbf{r}}_p - \bar{\mathbf{r}}_s))((\mathbf{r}_p - \mathbf{r}_s) - (\bar{\mathbf{r}}_p - \bar{\mathbf{r}}_s))^T] \\ &= E[(\Delta\mathbf{r}_p - \Delta\mathbf{r}_s)(\Delta\mathbf{r}_p - \Delta\mathbf{r}_s)^T] \\ &= E[(\Delta\mathbf{r}_p)(\Delta\mathbf{r}_p^T)] + E[(\Delta\mathbf{r}_s)(\Delta\mathbf{r}_s^T)] - E[(\Delta\mathbf{r}_p)(\Delta\mathbf{r}_s^T)] - E[(\Delta\mathbf{r}_s)(\Delta\mathbf{r}_p^T)] \,. \end{aligned} \tag{9}$$

Under the assumption of uncorrelated uncertainties, the relative position covariance matrix is the sum of the covariance matrices of the two objects

$$C = C_p + C_s \,, \tag{10}$$

since

$$E[(\Delta\mathbf{r}_p)(\Delta\mathbf{r}_s^T)] = E[(\Delta\mathbf{r}_p)]E[(\Delta\mathbf{r}_s^T)] = 0 \,. \tag{11}$$

In order to express the covariance matrices in the same reference frame, being R_{ps} the rotation matrix from the frame C_p is expressed in, to the C_s frame, the required computation is

$$C = C_p + R_{ps}^T C_s R_{ps} \,. \tag{12}$$

The covariance matrix of a three-dimensional distribution of random variables may be expressed as

$$C = \begin{bmatrix} \sigma_x^2 & \rho_{xy}\sigma_x\sigma_y & \rho_{xz}\sigma_x\sigma_z \\ \rho_{xy}\sigma_x\sigma_y & \sigma_y^2 & \rho_{yz}\sigma_y\sigma_z \\ \rho_{xz}\sigma_x\sigma_z & \rho_{yz}\sigma_y\sigma_z & \sigma_z^2 \end{bmatrix} , \tag{13}$$

Where ρ_{ij} is the correlation coefficient, defined as

$$\rho_{ij} = \frac{C_{ij}}{\sigma_i \sigma_j} \,, \tag{14}$$

and σ is the standard deviation, a quantity that quantify the amount of dispersion of a set of data, and it is defined as the square root of the variance σ^2

$$\sigma_x^2 = E[\Delta x \Delta x^T] \,. \tag{15}$$

The confidence region allows us to immediately visualize the errors associated to certain quantities. It is the multi-dimension version of the confidence interval, and in the three-dimensional case of a spacecraft's position, it is an ellipsoid

representing the space where, within a certain degree of confidence, the spacecraft is expected to be. It is defined by the equation

$$(\mathbf{x} - \boldsymbol{\mu}_{\mathbf{x}})^{\mathsf{T}} \mathbf{C}^{-1} (\mathbf{x} - \boldsymbol{\mu}_{\mathbf{x}}) \leqslant \chi^2 \,, \tag{16}$$

where χ is the quantile function associated to a determinate probability value p: values will fall inside the error ellipsoid p-percent of the time.

For almost circular orbits, the velocities of the objects of interest are aligned with the principal major axes of the respective ellipses [7]. As a consequence, the intermediate axis is aligned in the cross-track direction, and the minor axis in the radial direction. This assumption holds for the whole dissertation.

2.2.2 *B-plane*

It is useful now to introduce the b-plane, a coordinate system that is adopted to to compute both the miss distance and the collision probability.

The b-plane is illustrated in Figure 1, and it is defined as follows. The origin of the axes lies at the centre of the secondary object at the time of closest approach; the η-axis is defined along the direction of the relative velocity of the first satellite with respect to the secondary object; the $\xi\zeta$ plane is perpendicular to that η-axis.

$$\hat{\mathbf{u}}_{\xi} = \frac{\boldsymbol{v}_{\mathrm{s}} \times \boldsymbol{v}_{\mathrm{p}}}{\|\boldsymbol{v}_{\mathrm{s}} \times \boldsymbol{v}_{\mathrm{p}}\|} \,, \tag{17}$$

$$\hat{\mathbf{u}}_{\eta} = \frac{\boldsymbol{v}_{\mathrm{p}} - \boldsymbol{v}_{\mathrm{s}}}{\|\boldsymbol{v}_{\mathrm{p}} - \boldsymbol{v}_{\mathrm{s}}\|} \,, \tag{18}$$

$$\hat{\mathbf{u}}_{\zeta} = \hat{\mathbf{u}}_{\xi} \times \hat{\mathbf{u}}_{\eta} \,. \tag{19}$$

The position on the b-plane of the primary satellite at the time of closest approach

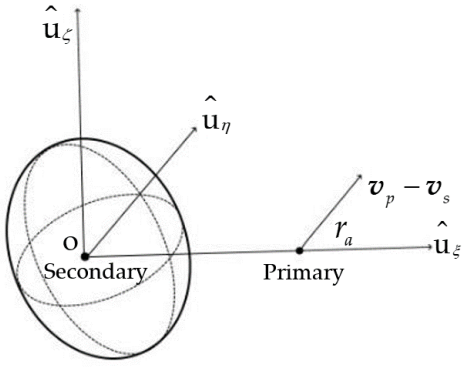

Figure 1: B-plane reference frame.

is then $\mathbf{r_b} = (\xi, 0, \zeta)$, and the miss distance can be computed as

$$\mathrm{d} = \sqrt{\xi^2 + \zeta^2} \,. \tag{20}$$

An impact can be direct or non-direct: an impact is called direct when the miss distances is zero, that is $\mathbf{r_b} = 0$, and it is called non-direct when, at the time of closest approach, the miss distance is different from zero.

2.2.3 *Short-term encounter approximation*

The hypothesis of short-term encounter approximation lays the basis for the analytical result that will be obtained for the computation of the collision probability. Under this hypothesis, the relative motion of the two objects of interest can be considered rectilinear: because of the high relative velocity, the primary spacecraft spends a really short time in the encounter region; consequently, the gravitational forces can be neglected and the combined covariance matrix can be considered constant.

An encounter can be considered short-term when the time t the primary satellite takes to cross the 1σ combined error ellipsoid is much smaller with respect to its orbital period T [6]

$$\epsilon = \frac{t}{T} \ll 1\,, \tag{21}$$

where t can be computed as

$$t = \frac{2\sigma_\eta}{\|\boldsymbol{v}_p - \boldsymbol{v}_s\|}\,. \tag{22}$$

This hypothesis is valid for most of the encounters, especially in Low Earth Orbits (LEOs). A detailed treatment about its validity can be found in [7].

2.2.4 *Computation of the collision probability*

In this section, the approach used in [7] to obtain an analytical expression for the collision probability is illustrated.

Assuming the two objects as spherical, let's denote with r_p the radius of the primary spacecraft and with r_s the radius of the secondary object. If the secondary object enters a sphere of radius $r_A = r_p + r_s$ centred at the primary, a collision happens.

Studying the motion of two spheres with the associated errors, is equivalent to study the relative motion of a sphere with radius equal to the sum of the radii of the single spheres (the primary satellite) with respect to a point mass (the secondary object) subjected to all the uncertainties. Defining for simplicity (x, y, z) the coordinates along the $(\hat{\mathbf{u}}_\zeta, \hat{\mathbf{u}}_\eta, \hat{\mathbf{u}}_\xi)$ axes, and therefore being $\mathbf{r} = [x, y, z]$ the relative position vector, assuming a three-dimensional Gaussian distribution of the uncertainties, the PDF of $\mathbf{r}$ is

$$f_3(x, y, z) = \frac{1}{\sqrt{(2\pi)^3 \|C\|}} e^{-\frac{1}{2}\mathbf{r}^T C^{-1}\mathbf{r}}\,, \tag{23}$$

where C is the combined covariance matrix.
The probability of collision is

$$P = \iiint_V f_3(x, y, z)\,dx\,dy\,dz\,, \tag{24}$$

where V is the volume swept by the sphere of radius r_A centred at the primary as it moves through the space of random variables (x, y, z) [7].

Making now the short-term encounter hypothesis, it is possible to reduce the volume integral to a double integral: assuming the motion rectilinear in the relative velocity direction, and being the standard deviation in the y-direction several kilometres, so that the motion is rectilinear over a region long several standard deviations, the volume swept by the sphere can be considered as a long cylinder extending in the y-direction from $-\infty$ to $+\infty$.

$$P = \iint_A f_2(x, z)\,dx\,dz\,, \tag{25}$$

where $f_2(x, z)$ is the bivariate Gaussian distribution and A is the collision circular cross-sectional area of radius r_A

$$f_2(x, z) = \frac{1}{2\pi\sigma_x\sigma_z\sqrt{1-\rho_{xz}^2}} e^{\frac{-\left[\left(\frac{x}{\sigma_x}\right)^2 - 2\rho_{xz}\left(\frac{x}{\sigma_x}\right)\left(\frac{z}{\sigma_z}\right) + \left(\frac{z}{\sigma_z}\right)^2\right]}{2(1-\rho_{xz}^2)}}\,. \tag{26}$$

The covariance matrix associated to this problem is

$$C = \begin{bmatrix} \sigma_x^2 & \rho_{xz}\sigma_z\sigma_x \\ \rho_{xz}\sigma_z\sigma_x & \sigma_z^2 \end{bmatrix}. \tag{27}$$

Changing reference frame, it is possible to simplify the analysis. A rotation from (x, z) to (x', z') allows us to eliminate the off-diagonal terms of the covariance matrix, since this new reference frame axes are chosen to be aligned with the major and minor axes of the error ellipse. Therefore the new covariance matrix in this reference frame is

$$C' = \begin{bmatrix} \sigma_{x'}^2 & 0 \\ 0 & \sigma_{z'}^2 \end{bmatrix}, \tag{28}$$

and the rotation angle between the frames is

$$\theta = \frac{1}{2}\tan^{-1}\left[\frac{2\rho_{xz}\sigma_x\sigma_z}{(\sigma_x^2 - \sigma_z^2)}\right]. \tag{29}$$

From the invariance of the covariance matrix determinant

$$\sigma_{x'}\sigma_{z'} = \sqrt{1-\rho_{xz}^2}\,\sigma_x\sigma_z\,, \tag{30}$$

it is possible to express the PDF in the new reference frame, and the corresponding collision probability

$$f_2(x', z') = \frac{1}{2\pi\sigma_{x'}\sigma_{z'}} e^{-\left[\left(\frac{x'}{\sigma_{x'}}\right)^2 + \left(\frac{z'}{\sigma_{z'}}\right)^2\right]}\,, \tag{31}$$

$$P = \iint_{A'} f_2(x', z')\,dx'\,dz'\,, \tag{32}$$

with

$$A' = A\,, \qquad r_{A'} = r_A\,, \qquad x_p' = x_e\cos\theta\,, \qquad z_e' = x_e\sin\theta\,, \tag{33}$$

and (x'_p, z'_p) denotes the new coordinates of the primary spacecraft in the b-plane. In order to develop the analytical expression of the collision probability, another change of coordinates is necessary, where the PDF is transformed into a isotropic function. This is accomplished with the coordinate change:

$$x'' = \frac{\sigma_{z'}}{\sigma_{x'}} x' ,$$

$$z'' = z' , \tag{34}$$

that maps the ellipses of constant PDF

$$\frac{x'^2}{\sigma_{x'^2}} + \frac{z'^2}{\sigma_{z'^2}} = k^2 , \tag{35}$$

into circles of constant PDF

$$\frac{x'^2}{\sigma_{z'^2}} + \frac{z'^2}{\sigma_{z'^2}} = k^2 . \tag{36}$$

Therefore, now the pdf is

$$f_3(x'', z'') = \frac{1}{2\pi\sigma_{z'^2}} e^{-\left(\frac{x''+z''}{2\sigma_{z'^2}}\right)} , \tag{37}$$

so that we have

$$A'' = \frac{\sigma_{z'}}{\sigma_{x'}} A' , \qquad a = r_{A'} , \qquad b = \frac{\sigma_{z'}}{\sigma_{x'}} r_{A'} , \tag{38}$$

with a, b semimajor axis and semi-minor axis of the new elliptical cross-sectional collision area. In order to proceed, it is necessary to approximate the elliptical cross section A'' with a circular cross section A''' of the same area with radius $r_{A'''}$. The new quantities then are

$$A''' = \pi r_{A'''}{}^2 , \qquad r_{A'''} = \sqrt{ab} , \qquad r''^2_p = x''^2_p + z''^2_p , \tag{39}$$

with r''_p distance of the primary satellite from the origin of the (x'', z'') coordinate system. The previous approximation allows us to transform the 2 dimensional isotropic pdf integrated over a circle of radius $r_{A'''}$ at distance r''_p from the origin into a one dimensional Rician pdf integrated from 0 to $r_{A'''}$

$$P = \int_0^{r_{A'''}} \frac{r}{\sigma^2_{z'}} \exp\left\{ -\frac{(r^2 + r''^2_p)}{2\sigma^2_{z'}} \right\} I_0\left(\frac{r r''_p}{\sigma^2_{z'}} \right) dr , \tag{40}$$

where $I_0(\cdot)$ is the modified Bessel function of the first kind of order zero. The analytical solution consists in an infinite series

$$P = e^{-\frac{v}{2}} \sum_{m=0}^{\infty} \frac{v^m}{2^m m!} \left[1 - e^{-\frac{u}{2}} \sum_{k=0}^{m} \frac{u^k}{2^k k!} \right] , \tag{41}$$

where the dimensionless variables u and v are defined as:

$$u = \left(\frac{r_A}{\sigma_{x'}\sigma_{z'}}\right)^2 = \left(\frac{r_A}{\sigma}\right)^2 , \tag{42}$$

$$v = \left(\frac{x_e}{\sigma^*}\right)^2 , \tag{43}$$

$$\sigma^{*2} = {\sigma_{z'}}^2 \left[1 + \left[\left(\frac{\sigma_{z'}}{\sigma_{x'}}\right)^2 - 1\right]\left(\frac{{x'_p}^2}{{x'_p}^2 + {z'_p}^2}\right)\right]^{-1} . \tag{44}$$

Retaining only the first term of the series, the collision probability can be expressed as

$$P = e^{-\frac{v}{2}}(1 - e^{-\frac{u}{2}}) + E_1 , \tag{45}$$

where E_1 is the truncation error, and it satisfies

$$E_1 < \frac{1}{8}u^2 v e^{-\frac{v}{2}} e^{\frac{uv}{4}} . \tag{46}$$

This is a fundamental result: an analytical expression that relates collision probability and miss distance, function only of the spacecraft position. This result is the foundation of this whole dissertation, as it is shown in 3.2, where the collision probability minimization problem is formulated.

2.3 OPTIMAL CONTROL THEORY

In the following section the general formulation of an Optimal Control Problem (OCP) is introduced, followed by the derivation of the solutions for the specific energy/fuel optimal problems.

OCP is a problem that consists in finding the functions $\mathbf{u}(t)$ that minimize (or maximize) a performance index J. The resolutive methods can be divided in two classes: *indirect methods*, which exploit the analytical optimality conditions arising from the calculus of variations, and *direct methods*, which convert the continuous optimal control problem into a parameter optimization problem [9].

This dissertation deals extensively with the indirect optimization problem, where the objective function is expressed in the Bolza form. The problem is formulated as follows:
minimizing(or maximizing) J

$$J = \Phi(t_f, \mathbf{x}_f) + \int_{t_0}^{t_f} L(t, \mathbf{x}, \mathbf{u})dt , \tag{47}$$

subjected to

$$\dot{\mathbf{x}} = \mathbf{f}(t, \mathbf{x}, \mathbf{u}) \,, \tag{48}$$

$$\mathbf{x}(t_i) = \mathbf{x}_i \,, \tag{49}$$

$$\boldsymbol{\Psi}(t_f, \mathbf{x}_f) = \mathbf{0} \,. \tag{50}$$

$$\tag{51}$$

The dynamical system under investigation is described by the differential equations (48), where $\mathbf{x}$ is the n-dimensional state vector, determined by the m-dimensional control vector $\mathbf{u}$.

In order to solve this problem, the Euler-Lagrange theorem is invoked: it states that, assuming $\Phi, L, f, \Psi \in C^1$ on their respective domains and that the optimal control, $u^* \in C^0[t_i, t_f]$, is unconstrained, there exists a time-varying multiplier vector $\boldsymbol{\lambda}^T(t) = (\lambda_1, \lambda_2, \cdots, \lambda_n)$ and a constant multiplier vector $\boldsymbol{\nu}^T = (\nu_1, \nu_2, \cdots, \nu_q)$ such that with the Hamiltonian

$$H(t, \mathbf{x}, \mathbf{u}, \boldsymbol{\lambda}) = L(t, \mathbf{x}, \mathbf{u}) + \boldsymbol{\lambda}^T \mathbf{f}(t, \mathbf{x}, \mathbf{u}) \,, \tag{52}$$

and a terminal function

$$\boldsymbol{\Phi}(t_f, \mathbf{x}_f) = \Phi(t_f, \mathbf{x}_f) + \boldsymbol{\nu}^T \boldsymbol{\Psi}(t_f, \mathbf{x}_f) \,, \tag{53}$$

the following necessary conditions must hold:

$$\dot{\boldsymbol{\lambda}}^T = -\frac{\partial H^*}{\partial \mathbf{x}} = -H_x^* \,, \tag{54}$$

$$\boldsymbol{\lambda}^T(t_f) = \frac{\partial \phi^*}{\partial \mathbf{x}_f} \,, \tag{55}$$

$$H_u^* = \mathbf{0}^T \,, \tag{56}$$

and the transversality condition:

$$\Omega(t_f, \mathbf{x}_f, \mathbf{u}_f) = L_f^* - \frac{d\Phi^*}{dt_f} = 0 \,, \tag{57}$$

which applies if t_f is unspecified [19].

It is worth to show the demonstration of this results, since it gives some useful insights of the problem. Re-writing J as

$$J = \Phi(t_f, \mathbf{x}(t_f)) + \int_{t_i}^{t_f} \left\{ H - \boldsymbol{\lambda}^T \dot{\mathbf{x}} \right\} dt \,, \tag{58}$$

and differentiating it with respect to the variations in the control vector $\mathbf{u}$, after a few manipulations [19], the final equation is set equal to 0, in order to find a stationary point of the cost J, necessary condition for a minimum

$$dJ = \frac{\partial \Phi^*}{\partial t_f} dt_f + \frac{\partial \Phi^*}{\partial \mathbf{x}_f} d\mathbf{x}_f + L^*(t_f^*) dt_f + \\ + \int_{t_i}^{t_f^*} \left[H_x^* \partial \mathbf{x}(t) + H_u^* \partial \mathbf{u}(t) - \boldsymbol{\lambda}^T(t) \partial \dot{\mathbf{x}}(t) \right] dt = 0 . \quad (59)$$

Integrating the last term by part

$$\int_{t_i}^{t_f^*} -\boldsymbol{\lambda}^T(t) \partial \dot{\mathbf{x}}(t) dt = \left[-\boldsymbol{\lambda}^T(t) \partial \mathbf{x}(t) \right] \Big|_{t_i}^{t_f^*} + \int_{t_i}^{t_f^*} \dot{\boldsymbol{\lambda}}^T(t) \partial \mathbf{x}(t) dt , \quad (60)$$

inserting (60) in (59), substituting $\partial \mathbf{x}(t_f^*) = d\mathbf{x}_f - \dot{\mathbf{x}}_f^* dt_f$ [19] and considering the initial time fixed, so that $\partial \mathbf{x}(t_i) = 0$

$$dJ = \left[\frac{\partial \Phi^*}{\partial t_f} + L^*(t_f^*) + \boldsymbol{\lambda}^T(t_f^*) \partial \dot{\mathbf{x}}_f^* \right] dt_f + \left[\frac{\partial \Phi^*}{\partial \mathbf{x}_f} - \boldsymbol{\lambda}^T(t_f^*) \right] d\mathbf{x}_f + \\ + \int_{t_i}^{t_f^*} \left\{ \left[H_x^* + \dot{\boldsymbol{\lambda}}^T \right] \partial \mathbf{x}(t) + H_u^* \partial \mathbf{u}(t) \right\} dt = 0 . \quad (61)$$

Exploiting now the arbitrarity of $\partial \mathbf{x}(t)$ and $\partial \mathbf{u}$, and the fact that dJ has to be zero for all $d\mathbf{x}(t_f)$ and dt_f, we finally obtain the set of equations (54)-(57). The set of equations (54) describes the dynamics of the costates, quantities without a clear physical meaning, that have to be integrated simultaneously with the state equations in order to obtain the optimal control law.

Instead of setting $\partial \mathbf{x}(t_i) = 0$ in (60), i.e. considering $\partial \mathbf{x}(t_i) \neq 0$, dJ would be zero only if $\boldsymbol{\lambda}^T(t_i) = 0$. This means that the optimal value of $x(t_i)$ is obtained when the corresponding costate $\lambda(t_i) = 0$. This allows us to draw a conclusion on the meaning of the costates: they represent the first-order sensitivity of a change in the cost function due to a variation in the initial state; since every time t can be considered as initial time, this conclusion applies at any time t, and that's why they are also called *influence functions* on J in variations in $\mathbf{x}(t)$[15]

Boundary Conditions (BCs) are split into initial and final ones: in order to solve this problem, it is necessary to solve a Two Boundary Value Problem (TPBVP). Several numerical techniques exist for this purpose; among them, the most famous is probably the shooting method, that certainly is the most intuitive one: the problem is translated in an initial value problem, and the trajectory is "shooted" until the tolerances on the BCs are respected. Other methods are finite-difference methods [12] and collocation methods, where the latter are the selected algorithms by Matlab® to solve TPBVP: the integration interval is divided into a mesh, and a set of algebraic equation resultant from the boundary conditions is solved. From the resultant error the mesh is adapted and the process is repeated [26].

2.3.1 *Fuel optimal formulation*

For minimum-fuel formulations, the cost function is defined as

$$J = \int_{t_0}^{t_f} L dt, \qquad L = \frac{T_{max}}{c_e} u \,. \tag{62}$$

The non-linear set of equations that describes our problem is 4, so the Hamiltonian becomes:

$$H = \boldsymbol{\lambda}_r^T \cdot \boldsymbol{v} + \boldsymbol{\lambda}_v^T \cdot \left(-\frac{\mu}{r^3}\mathbf{r} + T_{max}\frac{u}{m}\boldsymbol{\gamma} \right) + \frac{u T_{max}}{I_{sp} g_0}[1 - \lambda_m] \,, \tag{63}$$

where $\lambda_r, \boldsymbol{\lambda}_v, \lambda_m$ are the costates associated to position, velocity and mass, and u and $\boldsymbol{\gamma}$ are the thrust magnitude and direction, which represent the control law we are interested in.

The optimal control law is immediately retrieved applying the Potryagin minimum principle, which states that the Hamiltonian must be minimized over the set of all admissible $\mathbf{u}$ [15]. As a consequence, from (63) it is possible to see that the thrust direction must be in the same direction of $-\boldsymbol{\lambda}_v$, termed by Lawden [17] *primer vector*[1]

$$\boldsymbol{\gamma} = -\frac{\boldsymbol{\lambda}_v}{\|\boldsymbol{\lambda}_v\|} \,. \tag{64}$$

Therefore, H can be rewritten as

$$H = \boldsymbol{\lambda}_r^T \cdot \boldsymbol{v} + \boldsymbol{\lambda}_v^T \cdot \left(-\frac{\mu}{r^3}\mathbf{r} \right) + \frac{u T_{max}}{c_e} S_f \,, \tag{65}$$

where

$$S_f = 1 - c_e \frac{\|\boldsymbol{\lambda}_v\|}{m} - \lambda_m \tag{66}$$

is the Switching function.
Applying a second time the Minimum Principle [1], it is possible to find the optimal value of u, the only decision variable left unsorted. The resultant control law is

$$u = \begin{cases} 0 & \text{if} \quad S_f > 0 \,, \\ 0 \leqslant u \leqslant 1 & \text{if} \quad S_f = 0 \,, \\ 1 & \text{if} \quad S_f < 0 \,. \end{cases} \tag{67}$$

It can be seen that the optimal control law has a bang-bang profile: u depends only on the sign of S_f, therefore the thrust switch from 0 to the maximum value and vice versa, depending on the sign of S_f.

1 Lawden, in a personal letter:

> In regard to the term 'primer vector', you are quite correct in your supposition. I served in the artillery during the war [World War II] and became familiar with the initiation of the burning of cordite by means of a primer charge. Thus, p = 1 is the signal for the rocket motor to be ignited.

Costates equations of motion are found from (54), and they result to be

$$\dot{\boldsymbol{\lambda}}^T = -\frac{\partial H^*}{\partial \mathbf{x}} = \begin{cases} \dot{\boldsymbol{\lambda}}_{\mathbf{r}} = \frac{\mu}{r^3}\boldsymbol{\lambda}_{\mathbf{v}} - \frac{3\mu \mathbf{r}\boldsymbol{\lambda}_{\mathbf{v}}}{r^5}\mathbf{r}\,, \\ \dot{\boldsymbol{\lambda}}_{\mathbf{v}} = -\boldsymbol{\lambda}_{\mathbf{r}}\,, \\ \dot{\lambda}_m = -\frac{T_{max} u}{m^2}\lambda_v\,, \end{cases} \tag{68}$$

since the gravity gradient matrix $\mathbf{G}(\mathbf{r}) = \frac{\partial \mathbf{g}(\mathbf{r})}{\partial \mathbf{r}}$ is computed as

$$\begin{aligned} \frac{\partial \mathbf{g}(\mathbf{r})}{\partial \mathbf{r}} &= \left[r^3 (-\mu \frac{\partial \mathbf{r}}{\partial \mathbf{r}}) + \mu \mathbf{r} \left(3r^2 \frac{\partial r}{\partial \mathbf{r}} \right) \right] \Big/ r^6 \\ &= \frac{\mu}{r^5} \left(3\mathbf{r}\mathbf{r}^T - r^2 I_3 \right)\,, \end{aligned} \tag{69}$$

where I_3 is the 3-dimensional identity matrix.

2.3.2 *Energy optimal formulation*

In minimum-energy formulations, the control is expressed in terms of acceleration, therefore the cost function is defined as

$$J = \int_{t_i}^{t_f} L dt, \qquad L = \frac{1}{2}\mathbf{a}_c^T \mathbf{a}_c\,, \tag{70}$$

where $\mathbf{a}_c$ is the control acceleration.

In this formulation, the mass is not included in the state variables, since its equation is decoupled from the other. Thus, in order to simplify the equations, it is considered separately:

$$\dot{\mathbf{x}} = \begin{cases} \dot{\mathbf{r}} = \mathbf{v}\,, \\ \dot{\mathbf{v}} = \mathbf{g}(\mathbf{r}) + \mathbf{a}_c\,. \end{cases} \tag{71}$$

The Hamiltonian is

$$H = \boldsymbol{\lambda}_{\mathbf{r}}{}^T \mathbf{v} + \boldsymbol{\lambda}_{\mathbf{v}}{}^T \left(-\frac{\mu}{r^3}\mathbf{r} + \mathbf{a}_c \right) + \frac{1}{2}\mathbf{a}_c^T \mathbf{a}_c\,, \tag{72}$$

and the equations of motion for the costate are derived from (54)

$$\dot{\boldsymbol{\lambda}}^T = \begin{cases} \dot{\boldsymbol{\lambda}}_{\mathbf{r}} = \frac{\mu}{r^3}\boldsymbol{\lambda}_{\mathbf{v}} - \frac{3\mu \mathbf{r}\boldsymbol{\lambda}_{\mathbf{v}}}{r^5}\mathbf{r}\,, \\ \dot{\boldsymbol{\lambda}}_{\mathbf{v}} = -\boldsymbol{\lambda}_{\mathbf{r}}\,. \end{cases} \tag{73}$$

The Pontryagin minimum principle states that the optimal control is the one that minimize the Hamiltonian. Therefore, by inspection of (72), the optimal control acceleration is

$$\mathbf{a}_c = -\boldsymbol{\lambda}_{\mathbf{v}}\,. \tag{74}$$

In order to improve the numerical efficiency of the code, variables are normalized: the normalization units chosen are the orbital radius $l_{ref} = R$, the initial mass of the spacecraft m_0, and the reference velocity $v_{ref} = \sqrt{\frac{\mu}{R}}$, so that the reference time results $t_{ref} = \frac{v_{ref}}{l_{ref}}$.

2.3.3 *Continuation method*

The discontinuous solution resulted from the bang-bang optimal thrust profile is numerically difficult to obtain, hence a *continuation method* is adopted in order to improve the numerical solution process and help convergence.

Generally, a continuation method is used to obtain the solution of a complex problem by building a sequence of (simpler) auxiliary problems that converges to the original one [28].

The approach chosen in this work to bypass the problem, is the one illustrated in [24], where the discontinuous control law is approximated by exponential or arc-tangential C^∞ functions.

$$u = \frac{1}{1 + \exp(2S_f p)}, \qquad u = \frac{1}{2} + \frac{1}{\pi} \arctan -S_f p, \tag{75}$$

where p is the *continuation parameter*. Increasing the value of p, the behaviour of the bang-bang control law is slowly approximated through an iterative process, as shown in Figure 2. Each solution is used as initial guess for the p_{k+1} iteration, until the discontinuous profile is adequately approximated: at this point it is possible to integrate the equations of motion with the optimal discontinuous control law.

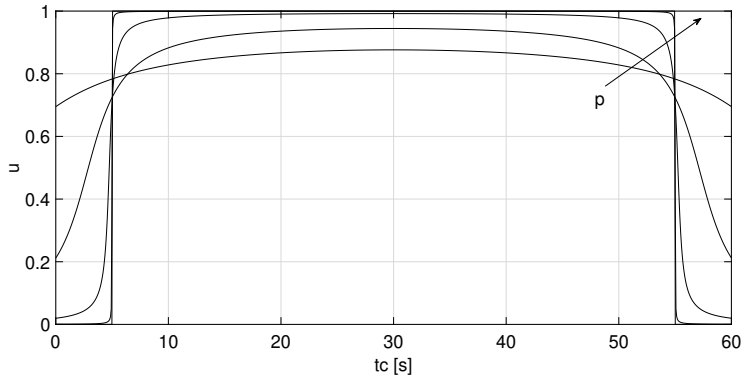

Figure 2: Continuation method.

2.4 OPTIMAL IMPULSIVE COLLISION AVOIDANCE MANOEUVRE

In this section the analytical optimal impulsive collision avoidance manoeuvre developed by [6] is illustrated, since it is the basis for the finite-burn conversion illustrated in Section 3.1 and it enlightens some important aspects about the collision probability computation that are going to be used in Section 3.5 for the formulation of the analytical approach.

The manoeuvre impulse $\Delta\boldsymbol{v}$ performed at an angular distance $\Delta\theta$ from the expected collision can be related to the displacement in the b-plane by the linear relation provided by [5]

$$\mathbf{r} = RKD\Delta\boldsymbol{v} = M\Delta\boldsymbol{v}\,, \tag{76}$$

where R, D, and K are the rotation, kinematics, and dynamics matrices. From equation (41) it is possible to notice that the collision probability P decreases exponentially with the variable v; as a consequence, in the case of direct impact, the optimization problem can be stated as: maximizing J

$$J = \left(\frac{\zeta}{\sigma_\zeta}\right)^2 + \left(\frac{\xi}{\sigma_\xi}\right)^2 - 2\rho_{\xi\zeta}\frac{\xi\zeta}{\sigma_\zeta\sigma_\xi}\,, \tag{77}$$

subjected to

$$f(\Delta\boldsymbol{v}) = \Delta\boldsymbol{v}^T\Delta\boldsymbol{v} - \Delta v_0^2\,, \leqslant 0 \tag{78}$$

where ξ, ζ are the coordinates along the b-plane axes $\hat{\mathbf{u}}_\xi, \hat{\mathbf{u}}_\zeta$. Defining the matrix Q^* as

$$Q^* = \begin{bmatrix} \frac{1}{\sigma_\zeta^2} & 0 & \frac{-\rho_{\xi\zeta}}{\sigma_\zeta\sigma_\xi} \\ 0 & 0 & 0 \\ \frac{-\rho_{\xi\zeta}}{\sigma_\zeta\sigma_\xi} & 0 & \frac{1}{\sigma_{\xi^2}} \end{bmatrix}\,, \tag{79}$$

the cost function can be rewritten as

$$J = \mathbf{r}^T Q^* \mathbf{r}\,. \tag{80}$$

Using (76), it is re-written as

$$J = \Delta\boldsymbol{v}^T M^T Q^* M\Delta\boldsymbol{v} = \Delta\boldsymbol{v}^T A^*\Delta\boldsymbol{v}\,. \tag{81}$$

The problem is solved through Lagrange multipliers, so writing the Lagrange function

$$L = J - \lambda f\,, \tag{82}$$

the necessary condition for a minimum is found through

$$\frac{\partial L}{\partial\Delta\boldsymbol{v}} = 2A\Delta\boldsymbol{v} - 2\lambda\Delta\boldsymbol{v} = 0\,. \tag{83}$$

The problem is reduced to an eigenvalue problem, where the optimal solution (the $\Delta\boldsymbol{v}$ direction) corresponds to the eigenvector $\mathbf{s}_1$ associated to the maximum eigenvalue. Therefore, the optimal impulse is

$$\Delta\boldsymbol{v}_{opt} = \Delta v_0 \mathbf{s}_1\,. \tag{84}$$

2.5 STATE TRANSITION MATRIX

In this section the theory behind the computation of the State Transition Matrix (STM) is briefly reviewed, and it is derived for the energy-optimal formulation, in order to set the basis for the understanding of the approaches developed in Section 3.5 and 3.6.

The state transition matrix $\Phi(t, t_0)$ allows us to map the variation of the state of a linear system at an arbitrary time t_0 into variation of the state at an arbitrary final time t. Considering a small variation δx_0 of the initial state, the solution at successive times can be expressed as

$$x(x_0 + \delta x_0, t) = x(x_0, t) + \delta x(t)\,, \tag{85}$$

and since the variations from the nominal trajectory are considered to be small, $x(x_0 + \delta x_0, t)$ can be expanded in Taylor series, so that (85) becomes

$$x(x_0, t) + \frac{\partial x}{\partial x_0}\delta x_0 + \cdots = x(x_0, t) + \delta x(t)\,. \tag{86}$$

The variation of δx with respect to δx_0 is the STM

$$\Phi(t, t_0) = \frac{\partial x}{\partial x_0}\,, \tag{87}$$

$$\delta x(t) = \Phi(t, t_0)\delta x(t_0)\,. \tag{88}$$

For time-varying systems, the STM is found by integrating

$$\dot{\Phi}(t, t_0) = A(t)\Phi(t, t_0)\,, \qquad \Phi(t_0, t_0) = I_{12\times 12}\,. \tag{89}$$

Where $A(t)$ is the state matrix of the linear system

$$\dot{x} = A(t)x\,. \tag{90}$$

In this case, we want to linearise the equations of motion $f(x, t)$ of the energy-optimal control problem around the nominal trajectory represented by the state x_n. The equations of motion and the state vector are

$$x = \begin{Bmatrix} r \\ v \\ \lambda_r \\ \lambda_v \end{Bmatrix}, \qquad \begin{cases} \dot{r} &= v\,, \\ \dot{v} &= -\frac{\mu}{r^3}r - \lambda_v\,, \\ \dot{\lambda}_r &= \frac{\mu}{r^3}\lambda_v - \frac{3\mu r \lambda_v}{r^5}r\,, \\ \dot{\lambda}_v &= -\lambda_r\,. \end{cases} \tag{91}$$

The nominal trajectory consists in the natural motion of the satellite around the Earth.

$$\begin{cases} \dot{r}_n &= v_n\,, \\ \dot{v}_n &= -\frac{\mu}{r_n^3}r_n\,, \\ \dot{\lambda}_{rn} &= 0\,, \\ \dot{\lambda}_{vn} &= 0\,. \end{cases} \tag{92}$$

Therefore, the state matrix

$$A = \left[\frac{\partial \mathbf{f}}{\partial \mathbf{x}}\right]\Bigg|_{\mathbf{x}_n} \tag{93}$$

results to be

$$A = \begin{bmatrix} \mathbf{0}_{3\times3} & \mathbf{I}_{3\times3} & \mathbf{0}_{3\times3} & \mathbf{0}_{3\times3} \\ -\mathbf{A}_{34} & \mathbf{0}_{3\times3} & \mathbf{0}_{3\times3} & -\mathbf{I}_{3\times3} \\ \mathbf{0}_{3\times3} & \mathbf{0}_{3\times3} & \mathbf{0}_{3\times3} & \mathbf{A}_{34} \\ \mathbf{0}_{3\times3} & \mathbf{0}_{3\times3} & -\mathbf{I}_{3\times3} & \mathbf{0}_{3\times3} \end{bmatrix}. \tag{94}$$

In particular

$$\mathbf{A}_{34} = \frac{\mu}{r_n^3}\mathbf{I}_{3\times3} + \begin{bmatrix} \frac{3\mu \mathbf{r}_n{}^2(1)}{r_n^5} & \frac{3\mu \mathbf{r}_n(1)\mathbf{r}_n(2)}{r_n^5} & \frac{3\mu \mathbf{r}_n(1)\mathbf{r}_n(3)}{r_n^5} \\ \frac{3\mu \mathbf{r}_n(2)\mathbf{r}_n(1)}{r_n^5} & \frac{3\mu \mathbf{r}_n{}^2(2)}{r_n^5} & \frac{3\mu \mathbf{r}_n(2)\mathbf{r}_n(3)}{r_n^5} \\ \frac{3\mu \mathbf{r}_n(3)\mathbf{r}_n(1)}{r_n^5} & \frac{3\mu \mathbf{r}_n(3)\mathbf{r}_n(1)}{r_n^5} & \frac{3\mu \mathbf{r}_n{}^3(1)}{r_n^5} \end{bmatrix}, \tag{95}$$

where $\mathbf{r}_n(1), \mathbf{r}_n(2)$ and $\mathbf{r}_n(3)$ are the components of the position vector on the nominal orbit $\mathbf{r}_n$, expressed in ECI.

3

PROPOSED METHODS

In this chapter four methods to design a continuous-thrust CAM are proposed, which have been developed in the perspective of finding a fast and reliable approach, suitable for on-board implementation. The objective to be minimized is the collision probability P_c at the time of closest approach, computed with (45). First a finite-burn conversion from an analytical impulsive optimal manoeuvre is implemented, following an indirect optimization method that relies on the theory of the optimal control problem. In Sections 3.3 and 3.4, the fuel/energy optimal control problem formulations are exploited, inserting the collision probability as terminal cost in the performance index J. These first two approaches rely on numerical methods, whose time consuming procedures and convergence problems may be a relevant drawback for their on-board implementation. Therefore, through the linearisation of the energy OCP and the use of the STM (2.5), two suitable procedures are obtained. In Section 3.5 an analytical approach is proposed, where in order to obtain the maximum decrease of the collision probability with the least deviation from the nominal trajectory, the direction of maximum change of P_c is exploited. The method proposed in Section 3.6 exploits the boundary conditions developed in Section 3.2.1, leading to a semi-analytical solution.

3.1 FINITE-BURN CONVERSION (FBC)

An exact impulsive to finite burn manoeuvre conversion is one that produces a finite burn solution whose final position and velocity state is equal to the final position and velocity of the original post impulsive manoeuvre at the time the finite burn manoeuvre ends [1].

As seen in Section 2.4, the method developed by [6] is a fast and simple way to compute the optimal impulsive Δv, therefore it is worth to investigate the results of a conversion to a finite-burn manoeuvre. The conversion is carried out by means of the indirect optimization method explained in [1], exploiting the fuel-optimal formulation.

The impulsive manoeuvre point is considered the middle point of the thrust arc, and the impulsive Δv is distributed over the arc bounded by the initial and final states, which are found by propagating backward and forward from the impulsive manoeuvre point over the pre-impulse and post-impulse trajectories. In order to find the ends of the thrust-arc, the burn time is estimated analytically. Since fuel/energy optimal transfers usually require longer time of flights to match the imposed boundary conditions, the Δt estimated is increased of an arbitrary percentile, chosen to be 20% [1].

$$\Delta t = \frac{c_e \Delta m}{T_{max}} + 1.2 \frac{c_e \Delta m}{T_{max}}, \tag{96}$$

where Δm is computed from the impulsive manoeuvre rocket equation

$$\Delta m = m_0 \left(e^{\|\Delta v\|/c_e} - 1 \right) . \tag{97}$$

The impulsive manoeuvre time t_0 is the midpoint of the finite burn arc, therefore initial and final burn time, t_i, t_f, are computed as

$$t_i = t_0 - \frac{\Delta t}{2} , \qquad t_f = t_0 + \frac{\Delta t}{2} . \tag{98}$$

Position and velocity are computed propagating the spacecraft state at t_0 backward on the pre-impulse trajectory and forward on the post-impulse trajectory.

Recalling the set of equations of motion of state and costate that describes the minimum-fuel control problem

$$\begin{cases} \dot{\mathbf{r}} = \boldsymbol{v} , \\ \dot{\boldsymbol{v}} = \mathbf{g}(\mathbf{r}) + T_{max} \frac{u}{m} \boldsymbol{\gamma} , \\ \dot{m} = -\frac{T_{max} u}{I_{sp} g_0} , \\ \dot{\boldsymbol{\lambda}}_{\mathbf{r}} = \frac{\mu}{r^3} \boldsymbol{\lambda}_{\boldsymbol{v}} - \frac{3 \mu \mathbf{r} \lambda_v}{r^5} \mathbf{r} , \\ \dot{\boldsymbol{\lambda}}_{\boldsymbol{v}} = -\boldsymbol{\lambda}_{\mathbf{r}} , \\ \dot{\lambda}_m = -\frac{T_{max} u}{m^2} \lambda_v , \end{cases} \tag{99}$$

and the optimal control law

$$u = \begin{cases} 0 & \text{if} \quad S_f > 0 , \\ 1 & \text{if} \quad S_f < 0 , \end{cases} \tag{100}$$

$$\boldsymbol{\gamma} = -\frac{\boldsymbol{\lambda}_{\boldsymbol{v}}}{\|\boldsymbol{\lambda}_{\boldsymbol{v}}\|} , \tag{101}$$

it is now necessary to specify the boundary conditions of this problem. $2n$ BCs, n number of state variables, are needed to have a well-posed TPBVP. Since position, velocity vector and mass are 7 variables, 14 BCs are necessary. Initial state and mass and final state give 13 boundary conditions, the missing one is represented by

$$\lambda_m(t_f) = 0 \tag{102}$$

since the final mass is free.

The resultant boundary conditions of the TPBVP therefore are

$$\boldsymbol{\Psi} = \begin{bmatrix} \mathbf{r}(t_i) - \mathbf{r}_i \\ \boldsymbol{v}(t_i) - \boldsymbol{v}_i \\ m(t_i) - m_i \\ \mathbf{r}(t_f) - \mathbf{r}_f \\ \mathbf{r}(t_f) - \mathbf{r}_f \\ \lambda_m(t_f) \end{bmatrix} . \tag{103}$$

The TPBVP is solved with the collocation method implemented in the Matlab® built-in function *bvp4c*. *bvp4c* is a finite difference code that implements the three-stage Lobatto IIIa formula. This method uses a collocation formula and the collocation polynomial provides a C1-continuous solution that is fourth-order accurate uniformly in $[t_i, t_f]$. Mesh selection and error control are based on the residual of the continuous solution [19].

Initial estimates for the variables are needed: the initial state in known, therefore it is necessary to provide an estimate of the initial costate. A proper initial guess can be retrieved directly from the knowledge of the impulsive $\Delta\boldsymbol{v}$, through the hypothesis that the initial thrust direction vector $\boldsymbol{\gamma}$ is equal to the impulsive manoeuvre direction.

$$\begin{cases} \boldsymbol{\gamma}(t_i) = \frac{\Delta\boldsymbol{v}}{\|\Delta\boldsymbol{v}\|}\,, \\ \\ \dot{\boldsymbol{\gamma}}(t_i) = \frac{\Delta\dot{\boldsymbol{v}}}{\|\Delta\boldsymbol{v}\|} - \frac{\Delta\boldsymbol{v}\cdot\Delta\dot{\boldsymbol{v}}}{\|\Delta\boldsymbol{v}\|^3}\Delta\boldsymbol{v}\,, \end{cases} \tag{104}$$

where

$$\Delta\dot{\boldsymbol{v}} = \Delta\boldsymbol{g} = \boldsymbol{g}(\boldsymbol{r}, \boldsymbol{v}^+, t_i) - \boldsymbol{g}(\boldsymbol{r}, \boldsymbol{v}^-, t_i) = \boldsymbol{0}\,, \tag{105}$$

$$\Delta\ddot{\boldsymbol{v}} = G_r\Delta\boldsymbol{v} + G_v\Delta\boldsymbol{g} = G_r\Delta\boldsymbol{v}\,, \tag{106}$$

$$G_r = \left[\frac{\partial\boldsymbol{g}}{\partial\boldsymbol{r}}\right]\,, \tag{107}$$

$$G_v = \left[\frac{\partial\boldsymbol{g}}{\partial\boldsymbol{v}}\right] = \boldsymbol{0}\,, \tag{108}$$

since $\boldsymbol{g}$ is function of the position $\boldsymbol{r}$ only (see (5)). At this point, according to [1], it is possible to compute the initial position and velocity costates estimation as

$$\boldsymbol{\lambda_v} = -\lambda_v\boldsymbol{\gamma}\,, \tag{109}$$

$$\boldsymbol{\lambda_r} = -\dot{\lambda}_v\boldsymbol{\gamma} + \lambda_v\dot{\boldsymbol{\gamma}} + \lambda_v G_v^T\boldsymbol{\gamma} = \boldsymbol{0}\,, \tag{110}$$

where, according to the primer vector theory, λ_v is estimated as

$$\lambda_v = \frac{T_{max}}{m_i}\,, \tag{111}$$

and the mass costate is estimated as

$$\lambda_{m_0} = c_e\left(\frac{1}{m_f} - \frac{1}{m_0}\right)\,. \tag{112}$$

The discontinuous control law requires the adoption of the continuation method introduced in Section 2.3.3. The discontinuous control law is approximated with the exponential function (75), and at every use of the function bvp4c the continuation parameter p is increased, until it is possible to converge to the discontinuous solution.

3.2 COLLISION PROBABILITY MINIMIZATION

The aim of this work is to provide a technique to compute a continuous-thrust manoeuvre that yields a reduction of the collision probability below a desired threshold, optimizing the propellant expenditure.

One possible way to accomplish the aforementioned goal, is by inserting the collision probability P_c computed with the Chan model (45) as terminal constraint into the cost function of the minimum-fuel formulation

$$J = P_c\left(t_f, \mathbf{x_f}\right) + \int_{t_i}^{t_f} \frac{T_{max}}{c_e} u dt\,, \tag{113}$$

where

$$\begin{aligned} P_c &= e^{-\frac{\nu}{2}}\left(1 - e^{-\frac{u}{2}}\right) \\ &= \exp\left\{\ln\left(1 - e^{-\frac{r_a^2}{2\sigma^2}}\right) - \frac{1}{2}\frac{d^2}{\sigma_\xi^2}\right\}. \end{aligned} \tag{114}$$

According to [25], σ^* from (44) can be simplified as $\sigma_{x'} = \sigma_\xi$ (expressed in the b-plane reference frame), and $\sigma = \sigma_\xi \sigma_\zeta$.

The miss distance d is computed as

$$d = \sqrt{\xi^2 + \zeta^2} = \left\| S R_b \left(\mathbf{r_f} - \mathbf{r_c}\right)\right\|^2, \qquad S = \begin{bmatrix} 1 & 0 & 0 \\ 0 & 0 & 0 \\ 0 & 0 & 1 \end{bmatrix}, \tag{115}$$

where R_b is the rotation matrix from the Earth Centred Inertial (ECI) reference frame to the b-plane, $\mathbf{r_c}$ and $\mathbf{r_f}$ are respectively the positions at the time of closest approach of the secondary object (where the b-plane is centred), and of the manoeuvrable spacecraft. In the case of a direct impact, the position of the primary and secondary objects at the time of closest approach coincides.

The collision probability appears to be function of the final position only: this allows us to analytically compute the necessary boundary conditions to have a well-posed TPBVP.

3.2.1 *Boundary conditions*

In the next approaches, the initial state is considered fixed. The optimization process is carried out by applying the optimization method for different manoeuvres points, in order to find not only the optimal manoeuvre for the manoeuvre point under investigation, but also perform a sensitivity analysis of the problem, which may yield to discover better optimal manoeuvre points along the orbit.

Being the initial state fixed, to have a well posed TPBVP, three or two additional boundary conditions are needed, depending on whether the minimum-fuel or minimum-energy formulation is under investigation. In the minimum-energy formulation the mass costate is not taken into account, since the mass is not a state

variable, being decoupled from the other equations of motion. The missing three boundary conditions are retrieved from (55), since $\Phi = P_c$. Recalling that

$$P_c = exp\left\{ ln\left(1 - e^{-\frac{r_a^2}{2\sigma^2}}\right) - \frac{1}{2}\frac{\|SR_b(\mathbf{r}_f - \mathbf{r}_c)\|^2}{\sigma_\xi^2} \right\}, \tag{116}$$

the costate final boundary conditions are

$$\frac{\partial \Phi}{\partial \mathbf{x}_f} = \begin{cases} \boldsymbol{\lambda}_{\mathbf{r}_f} = \frac{\partial \Phi}{\partial \mathbf{r}_f} = -\frac{1}{\sigma_\xi^2} R_b^T S^T \left(SR_b\left(\mathbf{r}_f - \mathbf{r}_c\right)\right) exp\left\{ ln\left(1 - e^{-\frac{r_a^2}{2\sigma^2}}\right) - \frac{1}{2}\frac{\|SR_b(\mathbf{r}_f - \mathbf{r}_c)\|^2}{\sigma_\xi^2} \right\}, \\ \boldsymbol{\lambda}_{\mathbf{v}_f} = \frac{\partial \Phi}{\partial \mathbf{v}_f} = 0, \\ \lambda_m = \frac{\partial \Phi}{\partial m_f} = 0. \end{cases} \tag{117}$$

The complete set of boundary conditions is collected in the vector $\boldsymbol{\Psi}$, where t_i is the initial time, and t_f is the final time, that is the time corresponding to the predicted closest approach:

$$\Psi = \begin{bmatrix} \mathbf{r}(t_i) - \mathbf{r}_i \\ \mathbf{v}(t_i) - \mathbf{v}_i \\ m(t_i) - m_i \\ \boldsymbol{\lambda}_{\mathbf{r}}(t_f) - \boldsymbol{\lambda}_{\mathbf{r}f} \\ \boldsymbol{\lambda}_{\mathbf{v}}(t_f) \\ \lambda_m(t_f) \end{bmatrix}. \tag{118}$$

3.2.2 *Weights on the Terminal Constraint*

This formulation of the problem gives no control on the resulting collision probability after manoeuvre execution. No threshold is specified: the final spacecraft state is the result of a trade-off between the path constraint that minimize the fuel or the energy and the terminal constraint on the collision probability. The relative relevance of these terms can be tuned by adding a weight W in the cost function J as

$$J = WP_c\left(t_f, \mathbf{x}_f\right) + \int_{t_i}^{t_f} \frac{T_{max}}{c_e} u dt, \qquad \text{(for minimum-fuel problems)}, \tag{119}$$

that directly affect the boundary condition on $\boldsymbol{\lambda}_{\mathbf{r}}$, being P_c a function of the final spacecraft position. Remembering that

$$P_c = exp\left\{ ln\left(1 - e^{-\frac{r_a^2}{2\sigma^2}}\right) - \frac{1}{2}\frac{\|SR_b(\mathbf{r}_f - \mathbf{r}_c)\|^2}{\sigma_\xi^2} \right\}, \tag{120}$$

the boundary condition on $\boldsymbol{\lambda}_{\mathbf{r}}$ is computed with (55), since $\Phi = WP_c$. Therefore

$$\boldsymbol{\lambda}_{\mathbf{r}_f} = -W\frac{1}{\sigma_\xi^2}R_b^T S^T \left(SR_b\left(\mathbf{r}_f - \mathbf{r}_c\right)\right) exp\left\{ ln\left(1 - e^{-\frac{r_a^2}{2\sigma^2}}\right) - \frac{1}{2}\frac{\left\|SR_b\left(\mathbf{r}_f - \mathbf{r}_c\right)\right\|^2}{\sigma_\xi^2}\right\}. \tag{121}$$

3.3 FUEL-OPTIMAL CONTROL PROBLEM (FOP)

As mentioned in Section 1.2, one of the most important features of a CAM is the efficiency in terms of propellant consumption. The fuel-optimal formulation illustrated in Section 2.3.1 grants a minimum-fuel solution to the minimization problem. Inserting P_c in the cost function as terminal cost, this formulation grants a solution that, according to the weights ratio between terminal and path cost (view Section 3.2.2), minimize P_c with the least amount of fuel.

P_c is inserted as terminal cost in the cost function J_f

$$J_f = P_c\left(t_f, \mathbf{x}_f\right) + \int_{t_i}^{t_f} \frac{T_{max}}{c_e} u dt, \tag{122}$$

associated to the equations of motion and the initial conditions

$$\dot{\mathbf{x}} = \begin{cases} \dot{\mathbf{r}} = \boldsymbol{v}, \\ \dot{\boldsymbol{v}} = -\frac{\mu}{r^3}\mathbf{r} - \frac{uT_{max}}{m}\boldsymbol{\gamma}, \\ \dot{m} = -\frac{uT_{max}}{c_e}, \end{cases} \qquad \text{ICs}: \begin{cases} \mathbf{r}(t_i) = \mathbf{r}_i, \\ \boldsymbol{v}(t_i) = \boldsymbol{v}_i, \\ m(t_i) = m_i. \end{cases} \tag{123}$$

The problem consists in finding the control parameters u and $\boldsymbol{\gamma}$, thrust ratio and direction, that minimize J_f. It translates in the solution of a TPBVP, whose boundary conditions are grouped in the vector $\boldsymbol{\Psi}$, and the equations of motion of state and costates are

$$\begin{cases} \dot{\mathbf{r}} = \boldsymbol{v}, \\ \dot{\boldsymbol{v}} = -\frac{\mu}{r^3}\mathbf{r} - \frac{uT_{max}}{m}\boldsymbol{\gamma}, \\ \dot{m} = -\frac{uT_{max}}{c_e}, \\ \dot{\boldsymbol{\lambda}}_{\mathbf{r}} = \frac{\mu}{r^3}\boldsymbol{\lambda}_{\boldsymbol{v}} - \frac{3\mu r \lambda_v}{r^5}\mathbf{r}, \\ \dot{\boldsymbol{\lambda}}_{\boldsymbol{v}} = -\boldsymbol{\lambda}_{\mathbf{r}}, \\ \dot{\lambda}_m = -\frac{T_{max}u}{m^2}\lambda_v, \end{cases} \qquad \boldsymbol{\Psi} = \begin{bmatrix} \mathbf{r}(t_i) - \mathbf{r}_i \\ \boldsymbol{v}(t_i) - \boldsymbol{v}_i \\ m(t_i) - m_i \\ \boldsymbol{\lambda}_{\mathbf{r}}(t_f) - \boldsymbol{\lambda}_{\mathbf{r}f} \\ \boldsymbol{\lambda}_{\boldsymbol{v}}(t_f) \\ \lambda_m(t_f) \end{bmatrix}. \tag{124}$$

The costate final BCs are

$$\boldsymbol{\lambda}(t_f) = \begin{cases} \boldsymbol{\lambda}_{\mathbf{r}_f} &= -\frac{1}{\sigma_\xi^2} R_b^T S^T \left(S R_b \left(\mathbf{r}_f - \mathbf{r}_c\right)\right) \exp\left\{ \ln\left(1 - e^{-\frac{r_a^2}{2\sigma^2}}\right) - \frac{1}{2} \frac{\|S R_b (\mathbf{r}_f - \mathbf{r}_c)\|^2}{\sigma_\xi^2} \right\}, \\ \boldsymbol{\lambda}_{\mathbf{v}_f} &= \mathbf{0}, \\ \lambda_m &= 0, \end{cases} \tag{125}$$

and the optimal control law resulting from the application of the Euler-Lagrange theorem and the Potryagin minimum principle is

$$u = \begin{cases} 0 & \text{if} \quad S_f > 0, \\ 0 \leqslant u \leqslant 1 & \text{if} \quad S_f = 0, \\ 1 & \text{if} \quad S_f < 0, \end{cases} \tag{126}$$

with

$$S_f = 1 - c_e \frac{\|\boldsymbol{\lambda}_v\|}{m} - \lambda_m \,. \tag{127}$$

The unknown boundary conditions to be retrieved are the initial costates $\boldsymbol{\lambda}(t_i)$. The discontinuous optimal control law (67) is numerically difficult to obtain, therefore the continuation method explained in Section 2.3.3 is applied. The control parameter u is approximated by the exponential function (75), and at each iteration the problem is solved thanks to the Matlab® built-in function *bvp4c*. Initial estimations of the variables need to be provided to the solver: in order to find appropriate costate' initial guesses, the Adjoint Control Transformation (ACT) developed in [23] is adopted.

3.3.1 *Adjoint Control Transformation*

Because of the lack of physical meaning of the costates, it is not easy to guess the values they could assume. The method developed by [23] provides an estimate of the position and velocity costates starting from the knowledge of the thrust direction, a variable that has a clear physical meaning and that can be more easily guessed.

The velocity costate is replaced by the thrust direction vector, and it is expressed in a vehicle-centred coordinate frame

$$\hat{\mathbf{v}} = \frac{\boldsymbol{v}}{v}, \tag{128}$$

$$\hat{\mathbf{h}} = \frac{(\mathbf{r} \times \boldsymbol{v})}{\|\mathbf{r} \times \boldsymbol{v}\|}, \tag{129}$$

$$\hat{\boldsymbol{w}} = \hat{\mathbf{h}} \times \hat{\mathbf{v}} \,. \tag{130}$$

The thrust direction and its derivative are expressed through the use of the angles α and β, as

$$\boldsymbol{\gamma}_{vwh} = \begin{bmatrix} \cos\alpha\cos\beta \\ \sin\alpha\cos\beta \\ \sin\beta \end{bmatrix}, \qquad \dot{\boldsymbol{\gamma}}_{vwh} = \begin{bmatrix} -\dot{\alpha}\sin\alpha\cos\beta - \dot{\beta}\cos\alpha\sin\beta \\ \dot{\alpha}\cos\alpha\cos\beta - \dot{\beta}\sin\alpha\sin\beta \\ \dot{\beta}\cos\beta \end{bmatrix}, \tag{131}$$

where

$$\alpha = \tan^{-1}\frac{\gamma_y}{\gamma_x}, \tag{132}$$

$$\beta = \tan^{-1}\frac{\gamma_x}{\sqrt{\gamma_x^2+\gamma_y^2}}, \tag{133}$$

$$\dot{\alpha} = \frac{\gamma_x\dot{\gamma}_y - \gamma_y\dot{\gamma}_x}{\sqrt{\gamma_x^2+\gamma_y^2}}, \tag{134}$$

$$\dot{\beta} = \tan^{-1}\frac{\dot{\gamma}_z}{\sqrt{\gamma_x^2+\gamma_y^2}}. \tag{135}$$

The guess for the thrust direction is the same as the one adopted in Section 3.1, therefore γ_x and γ_y are the components of $\boldsymbol{\gamma}$ computed in (104). It is now necessary to rotate $\boldsymbol{\gamma}_{vwh}$ and $\dot{\boldsymbol{\gamma}}_{vwh}$ in the Earth Centred Inertial reference frame, that is the one used to integrate the equations of motion.

$$\boldsymbol{\gamma}_{ijk} = R_{vwh-ECI}\boldsymbol{\gamma}_{vwh}, \tag{136}$$

$$\dot{\boldsymbol{\gamma}}_{ijk} = R_{vwh-ECI}\dot{\boldsymbol{\gamma}}_{vwh} + \dot{R}_{vwh-ECI}\boldsymbol{\gamma}_{vwh}. \tag{137}$$

The initial costates are finally estimated as

$$\boldsymbol{\lambda_v} = -\lambda_v\hat{\mathbf{u}}_{ijk}, \tag{138}$$

$$\dot{\boldsymbol{\lambda}}_v = -\dot{\lambda}_v\hat{\mathbf{u}}_{ijk} - \lambda_v\dot{\hat{\mathbf{u}}}_{ijk}, \tag{139}$$

$$\boldsymbol{\lambda_r} = -\dot{\boldsymbol{\lambda}}_{\boldsymbol{v}} - H^T\boldsymbol{\lambda_v}, \tag{140}$$

where λ_v is estimated as $\frac{T_{max}}{m_i}$, because of the result of the *primer vector theory*.

3.4 ENERGY-OPTIMAL CONTROL PROBLEM (EOP)

The FOP illustrated in the previous section is characterized by a discontinuous solution, the thrust profile has a bang-bang profile that could cause numerical difficulties in the integration of the equations of motion. Even relying on the continuation method, the problem is very sensitive on the increasing rate of the parameter p, and convergence issues could still arise. It is therefore interesting to examine the energy-optimal formulation explained in Section 2.3.2. Even if there is no bound on the control acceleration value, therefore no control on the

propellant mass, the continuous solution is appealing and makes this formulation worth investigating.

P_c is inserted as terminal cost in the cost function J_e,

$$J_e = P_c(t_f, \mathbf{x}_f) + \int_{t_i}^{t_f} \mathbf{a}_c^T \mathbf{a}_c \, dt \,. \tag{141}$$

The problem consists in finding the control acceleration $\mathbf{a}_c$ that minimizes J_e, subjected to the equations of motion and the initial conditions

$$\dot{\mathbf{x}} = \begin{cases} \dot{\mathbf{r}} = \mathbf{v} \,, \\ \dot{\mathbf{v}} = \frac{\mu}{r^3}\mathbf{r} + \mathbf{a}_c \,, \end{cases} \qquad \text{ICs} : \begin{cases} \mathbf{r}(t_i) = \mathbf{r}_i \,, \\ \mathbf{v}(t_i) = \mathbf{v}_i \,. \end{cases} \tag{142}$$

The mass is not included in the state variables, since its equation is decoupled from the other. In order to reduce the size of the problem, it is considered separately,

$$\dot{m} = -\frac{m}{c_e}\|\mathbf{a}_c\| \,. \qquad m(t_i) = m_i \,. \tag{143}$$

The problem translates in the solution of a TPBVP, whose boundary conditions are grouped in the vector $\boldsymbol{\Psi}$. The state and costate equations to be integrated simultaneously are

$$\begin{cases} \dot{\mathbf{r}} = \mathbf{v} \,, \\ \dot{\mathbf{v}} = \frac{\mu}{r^3}\mathbf{r} - \boldsymbol{\lambda}_v \,, \\ \dot{\boldsymbol{\lambda}}_r = \frac{\mu}{r^3}\boldsymbol{\lambda}_v - \frac{3\mu r \lambda_v}{r^5}\mathbf{r} \,, \\ \dot{\boldsymbol{\lambda}}_v = -\boldsymbol{\lambda}_r \,, \end{cases} \qquad \boldsymbol{\Psi} = \begin{bmatrix} \mathbf{r}(t_i) - \mathbf{r}_i \\ \mathbf{v}(t_i) - \mathbf{v}_i \\ \boldsymbol{\lambda}_r(t_f) - \boldsymbol{\lambda}_{rf} \\ \boldsymbol{\lambda}_v(t_f) \end{bmatrix} , \tag{144}$$

since the optimal control acceleration is

$$\mathbf{a}_c = -\boldsymbol{\lambda}_v \,. \tag{145}$$

The explicit conditions on the final costates are

$$\boldsymbol{\lambda}(t_f) = \begin{cases} \boldsymbol{\lambda}_{r_f} &= -\frac{1}{\sigma_\xi^2} R_b^T S^T \left(S R_b \left(\mathbf{r}_f - \mathbf{r}_c\right)\right) \exp\left\{ \ln\left(1 - e^{-\frac{r_a^2}{2\sigma^2}}\right) - \frac{1}{2}\frac{\|S R_b (\mathbf{r}_f - \mathbf{r}_c)\|^2}{\sigma_\xi^2} \right\} , \\ \boldsymbol{\lambda}_{v_f} &= 0 \,. \end{cases} \tag{146}$$

The initial costates $\boldsymbol{\lambda}(t_i)$ are found through the shooting method, and the optimal control law is computed through simple integration of the equations of motion.

3.4.1 *Shooting method*

The optimal control law of the EOP has a continuous profile, and no numerical difficulties arise from the adoption of the shooting method for its resolution. As already outlined, the method consists in guessing the initial costate, propagating the trajectory forward, checking the error on the final boundary conditions and through Newton iterations adjusting the initial costate, until the residual on the final boundary conditions is below a given threshold. The ACT (see Section 3.3.1) is used to find appropriate costates' initial guesses.

3.5 ANALYTICAL METHOD (AM)

In the first two methods the fuel and energy formulations of the OCP are exploited, leading to time consuming fully numerical iterative methods. In the perspective of finding a method that can be implemented onboard, the linearisation of the EOP formulated in Section 2.5 is exploited.

A CAM has to be efficient in terms of propellant, but also as compliant as possible with mission requirements. In the analytical approach presented here the direction of maximum change of P_c is exploited, in order to obtain the largest decrease of P_c with the least deviation possible from the nominal trajectory.

The cost function (80) formulated by [6] and illustrated in Section 2.4 exploits the same idea. The impulsive manoeuvre optimization is based on maximizing

$$J_{imp} = \mathbf{r}_b^T Q^* \mathbf{r}_b \,, \tag{147}$$

since P_c decreases exponentially with ν (41), where $\mathbf{r_b}$ is the position of the primary satellite on the b-plane at the time of closest approach.

In order to exploit the STM (94), it is now necessary to express J_{imp} in terms of deviations of the spacecraft from the nominal trajectory, since the STM maps the variations of the initial states into variations of the final state:

$$\begin{Bmatrix} \delta\mathbf{r_f} \\ \delta\mathbf{v_f} \\ \delta\boldsymbol{\lambda}_{\mathbf{r_f}} \\ \delta\boldsymbol{\lambda}_{\mathbf{v_f}} \end{Bmatrix} = \begin{bmatrix} \Phi_{11} & \Phi_{12} & \Phi_{13} & \Phi_{14} \\ \Phi_{21} & \Phi_{22} & \Phi_{23} & \Phi_{24} \\ \Phi_{31} & \Phi_{32} & \Phi_{33} & \Phi_{34} \\ \Phi_{41} & \Phi_{42} & \Phi_{43} & \Phi_{44} \end{bmatrix} \begin{Bmatrix} \delta\mathbf{r_0} \\ \delta\mathbf{v_0} \\ \delta\boldsymbol{\lambda}_{\mathbf{r_0}} \\ \delta\boldsymbol{\lambda}_{\mathbf{v_0}} \end{Bmatrix} . \tag{148}$$

In this approach the initial state is fixed, and the costates are zero on the nominal trajectory, therefore the following relations hold:

$$\mathbf{r}_0 = \mathbf{r}_m \rightarrow \delta\mathbf{r}_0 = \mathbf{r}_0 - \mathbf{r}_m = 0\,, \tag{149}$$

$$\mathbf{v}_0 = \mathbf{v}_m \rightarrow \delta\mathbf{v}_0 = \mathbf{v}_0 - \mathbf{v}_m = 0\,, \tag{150}$$

$$\boldsymbol{\lambda}_{\mathbf{r}_m} = 0 \rightarrow \delta\boldsymbol{\lambda}_{\mathbf{r}_0} = \boldsymbol{\lambda}_{\mathbf{r}_0}\,, \tag{151}$$

$$\boldsymbol{\lambda}_{\mathbf{v}_m} = 0 \rightarrow \delta\boldsymbol{\lambda}_{\mathbf{v}_0} = \boldsymbol{\lambda}_{\mathbf{v}_0}\,, \tag{152}$$

$$\delta\mathbf{r}_f = \mathbf{r}_f - \mathbf{r}_c\,, \tag{153}$$

$$\delta\mathbf{v}_f = \mathbf{v}_f - \mathbf{v}_c\,, \tag{154}$$

$$\boldsymbol{\lambda}_{\mathbf{r}_c} = 0 \rightarrow \delta\boldsymbol{\lambda}_{\mathbf{r}_f} = \boldsymbol{\lambda}_{\mathbf{r}_f}\,, \tag{155}$$

$$\boldsymbol{\lambda}_{\mathbf{v}_c} = 0 \rightarrow \delta\boldsymbol{\lambda}_{\mathbf{v}_f} = \boldsymbol{\lambda}_{\mathbf{v}_f}\,, \tag{156}$$

where $\mathbf{r}_m, \mathbf{v}_m, \boldsymbol{\lambda}_{\mathbf{r}_m}, \boldsymbol{\lambda}_{\mathbf{v}_m}$ are the state and costate at the initial manoeuvre point, that is at the initial time t_i; $\mathbf{r}_c, \mathbf{v}_c, \boldsymbol{\lambda}_{\mathbf{r}_c}, \boldsymbol{\lambda}_{\mathbf{v}_c}$ are the state and costate at the time of closest approach on the nominal trajectory, and $\mathbf{r}_f, \mathbf{v}_f, \boldsymbol{\lambda}_{\mathbf{r}_f}, \boldsymbol{\lambda}_{\mathbf{v}_f}$ are the state and costate at the time of closest approach after the manoeuvre.

As already mentioned in Section 2.2.2, the position in the b-plane of the manoeuvrable object is defined as

$$\mathbf{r}_b = R_b(\mathbf{r}_f - \mathbf{r}_{2_c})\,, \tag{157}$$

since the b-plane is centred in the secondary object, and $\mathbf{r}_{2_c}$ is the position of the non-manoeuvrable object at the time of closest approach, expressed in the same reference frame as $\mathbf{r}_f$. R_b is the rotation matrix to the b-plane.

In the case of direct impact, the position of the manoeuvrable satellite coincides with the one of the secondary object, $\mathbf{r}_{2_c} = \mathbf{r}_c$, therefore the position in the b-plane is

$$\mathbf{r}_b = R_b(\mathbf{r}_f - \mathbf{r}_c) = R_b\delta\mathbf{r}_f\,. \tag{158}$$

The problem can then be stated as maximizing

$$J_{AM} = \delta\mathbf{r}_f^T R_b^T Q^* R_b \delta\mathbf{r}_f\,, \tag{159}$$

subjected to the inequality constraint

$$\delta\mathbf{r}_f^T\delta\mathbf{r}_f - \delta\bar{\mathbf{r}}_f^2 \leqslant 0\,, \tag{160}$$

where the constraint (160) is applied in order to limit the variation from the nominal trajectory, being $\delta\bar{\mathbf{r}}_f$ a maximum arbitrary deviation. This minimization problem is solved through Lagrange multipliers, in the same way [6] solves the problem of the optimal impulsive CAM, explained in Section 2.4. Adjoining the constraint to the cost function, the Lagrangian is

$$L = \delta\mathbf{r}_f^T R_b^T Q^* R_b \delta\mathbf{r}_f - \lambda_{AM}(\delta\mathbf{r}_f^T\delta\mathbf{r}_f - \delta\bar{\mathbf{r}}_f^2)\,. \tag{161}$$

The necessary condition for a minimum is then

$$\frac{\partial L}{\partial \mathbf{r}_f} = 2R_b^T Q^* R_b \delta \mathbf{r}_f - 2\lambda_{SA} \delta \mathbf{r}_f = 0\,. \tag{162}$$

Equation (162) represent an eigenvalue problem

$$(R_b^T Q^* R_b - \lambda_{SA} I_3)\delta \mathbf{r}_f = 0\,, \tag{163}$$

where the direction $\mathbf{d}_{max}$ over which P_c changes more rapidly, is the eigenvector correspondent to the maximum eigenvalue $\lambda_{SA_{max}}$. Therefore, $\delta \mathbf{r}_f$ is imposed to be on this direction

$$\delta \mathbf{r}_f = \epsilon_{AM} \mathbf{d}_{max}\,, \tag{164}$$

and the final position of the spacecraft is $\mathbf{r}_f = \mathbf{r}_c + \delta \mathbf{r}_f$.
The final position of the spacecraft varies accordingly to ϵ_{AM}, and the resulting P_c is

$$P_c = exp\left\{ ln\left(1 - e^{-\frac{r_a^2}{2\sigma^2}}\right) - \frac{1}{2}\frac{\|SR_b(\delta \mathbf{r}_f)\|^2}{\sigma_\xi^2} \right\}. \tag{165}$$

Equation (165) provides a collision probability profile dependant on ϵ_{AM}. Chosen the desired P_c, the correspondent $\delta \mathbf{r}_f$ is computed and, thanks to the STM, the initial costates are retrieved. Since the final velocity is free, the associated final costate is zero. The initial position and velocity are fixed, therefore from the fourth row of (148)

$$\begin{aligned} 0 &= \Phi_{43} \delta \lambda_{r_0} + \Phi_{44} \delta \lambda_{v_0}\,, \\ \rightarrow \delta \lambda_{r_0} &= -\Phi_{43}^{-1} \Phi_{44} \delta \lambda_{v_0}\,. \end{aligned} \tag{166}$$

Once $\delta \mathbf{r}_f$ is known, it is possible to compute $\delta \lambda_{v0}$ and $\delta \lambda_{r0}$

$$\delta \mathbf{r}_f = \Phi_{13} \delta \lambda_{r_0} + \Phi_{14} \delta \lambda_{v_0} \tag{167}$$

$$= -\Phi_{13} \Phi_{43}^{-1} \Phi_{44} \delta \lambda_{v_0} + \Phi_{14} \delta \lambda_{v_0} \tag{168}$$

$$\rightarrow \delta \lambda_{v_0} = \left[-\Phi_{13} \Phi_{43}^{-1} \Phi_{44} + \Phi_{14}\right]^{-1} \delta \mathbf{r}_f\,. \tag{169}$$

All the initial conditions are now available, since $\delta \lambda_{r0} = \lambda_{r0}$ and $\delta \lambda_{v0} = \lambda_{v0}$. It is finally possible to integrate the equations of motion (144) and obtain the control law.

3.6 SEMI-ANALYTICAL METHOD (SAM)

This fourth approach starts from the linearisation of the EOP illustrated in Section 2.5. The final BCs of the TPBVP associated with the EOP are here exploited to find a direct relation between the applied weight W to the terminal cost and P_c,

$$J = W P_c(t_f, \mathbf{x}_f) + \int_{t_i}^{t_f} \mathbf{a}_c^T \mathbf{a}_c \, dt\,. \tag{170}$$

In this way it is possible to compute the weight to apply in order to obtain the control law to achieve a desired P_c. It is worth highlighting again that in the FBC and the FOP/EOP methods P_c is a result of the optimization, and it is not possible to know a-priori its value.

The aim here is to find a relation between W and $\delta\mathbf{r}_f$, since the collision probability depends only on the spacecraft position

$$P_c = \exp\left\{\ln\left(1-e^{-\frac{r_a^2}{2\sigma^2}}\right) - \frac{1}{2}\frac{\|SR_b(\delta\mathbf{r}_f)\|^2}{\sigma_\xi^2}\right\}, \tag{171}$$

where $\delta\mathbf{r}_f = \mathbf{r}_f - \mathbf{r}_c$.
The weight in the terminal cost affects the final conditions on the costates (146), that can be rewritten as

$$\begin{cases} \boldsymbol{\lambda}_{\mathbf{r}f} &= -W\frac{1}{\sigma_\xi^2}R_b^T S^T\left(SR_b\left(\delta\mathbf{r}_f\right)\right)\exp\left\{\ln\left(1-e^{-\frac{r_a^2}{2\sigma^2}}\right) - \frac{1}{2}\frac{\|SR_b(\delta\mathbf{r}_f)\|^2}{\sigma_\xi^2}\right\}, \\ \boldsymbol{\lambda}_{vf} &= 0. \end{cases} \tag{172}$$

The desired relation between $\mathbf{r}_f$ and W can be found by exploiting the STM (148). Remembering equations (149) and (150)

$$\delta\mathbf{r}_0 = 0, \tag{173}$$

$$\delta\mathbf{v}_0 = 0, \tag{174}$$

from equation (156), $\delta\boldsymbol{\lambda}_{vf} = \boldsymbol{\lambda}_{vf} = 0$, the same relation already computed in (166) is found

$$\delta\boldsymbol{\lambda}_{v0} = -\Phi_{44}^{-1}\Phi_{43}\delta\boldsymbol{\lambda}_{r0}. \tag{175}$$

Therefore, substituting (175) in the third row of (148) it is possible to obtain a relation between $\delta\boldsymbol{\lambda}_{r0}$ and $\delta\boldsymbol{\lambda}_{rf}$:

$$\delta\boldsymbol{\lambda}_{rf} = \Phi_{33}\delta\boldsymbol{\lambda}_{r0} + \Phi_{34}\delta\boldsymbol{\lambda}_{v0}, \tag{176}$$

$$= \left(\Phi_{33} - \Phi_{34}\Phi_{44}^{-1}\Phi_{43}\right)\delta\boldsymbol{\lambda}_{r0}, \tag{177}$$

$$= B\delta\boldsymbol{\lambda}_{r0}, \tag{178}$$

$$\rightarrow \delta\boldsymbol{\lambda}_{r0} = B^{-1}\delta\boldsymbol{\lambda}_{rf}. \tag{179}$$

It is now possible to write $\mathbf{r}_f$ as function of $\delta\boldsymbol{\lambda}_{rf}$,

$$\delta\mathbf{r}_f = \Phi_{13}\delta\boldsymbol{\lambda}_{r0} + \Phi_{14}\delta\boldsymbol{\lambda}_{v0}, \tag{180}$$

$$= \left(\Phi_{13} - \Phi_{14}\Phi_{44}^{-1}\Phi_{43}\right)\delta\boldsymbol{\lambda}_{r0}, \tag{181}$$

$$= C\delta\boldsymbol{\lambda}_{r0}, \tag{182}$$

$$= CB^{-1}\delta\boldsymbol{\lambda}_{rf}. \tag{183}$$

Remembering now that $\delta\boldsymbol{\lambda}_{\mathbf{r}f} = \boldsymbol{\lambda}_{\mathbf{r}f}$,

$$\delta\mathbf{r}_f = -WCB^{-1}\frac{1}{\sigma_\xi^2}R_b^T S^T S R_b \delta\mathbf{r}_f \exp\left\{\ln\left(1-e^{-\frac{r_a^2}{2\sigma^2}}\right) - \frac{1}{2}\frac{\|SR_b\delta\mathbf{r}_f\|^2}{\sigma_\xi^2}\right\}. \quad (184)$$

A set of three non-linear equations relating the spacecraft final position ($\mathbf{r}_f = \delta\mathbf{r}_f + \mathbf{r}_c$) to the terminal cost weight W has been found. The unknown variable to be computed is $\delta\mathbf{r}_f$, and the solution can be easily obtained trough Newton's iterations. $\mathbf{d}_{max}$, the direction of maximum change of P_c found in Section 3.5 through the eigenvalue problem (163), turns out to be an appropriate first guess (see Chapter 4). Once $\mathbf{r}_f$ is found, the correspondent P_c is computed with (165), and a probability profile for different manoeuvre points and weights is obtained.

4

NUMERICAL RESULTS

In this chapter the numerical results of the proposed methods developed in Chapter 3 are illustrated. First the test case is introduced. Afterwards, each method is individually tested and the particular features of each one are enlightened. In the last section, the methods are compared in terms of propellant consumption, computational time and robustness.

4.1 TEST CASE

The test case examined is the collision between the American communication satellite Iridium 33 and the derelict Russian communication satellite Cosmos 2251, happened on February 10^{TH}, 2009. The two satellites impacted at 789 km above the Tajmyr peninsula, in Russia, even if the predicted miss distance was of 584 m. It was not even the closest approach predicted for the Iridium satellites that week, but at the time the close approach was predicted, the satellite become silent, and a cloud of debris tracked by the US Space Surveillance Network confirmed the collision [16]. Following [6], the two satellites have been modelled as two spherical bodies respectively having a radius of 4 m and 3 m, such that the combined cross sectional radius results r_a =7 m. A covariance matrix with standard deviations of 0.1km in the tangential direction and 1km in the radial and out-of-plane directions has been assumed for both objects. The combined covariance matrix C_{uvw} expressed in the UVW reference frame of the manoeuvrable satellite is computed with (12); in order to express C_{uvw} in the b-plane reference frame, a final rotation is applied, $C = R_b^T C_{uvw} R_b$, and the resulting covariance matrix is

$$C = \begin{bmatrix} 0.02\text{km}^2 & 0 \\ 0 & 0.8\text{km}^2 \end{bmatrix}. \tag{185}$$

The orbits of the two satellites are assumed to be circular, which is a reasonable assumptions since the eccentricities are of the order of 10^{-5}. Since for circular orbits the argument of periapsis ω is not defined, in order to alter the least possible the real orbital elements it was chosen to maintain the original argument of periapsis value for both the orbits. The orbital parameters are listed in Table 1, where the set $a_i, e_i, i_i, \Omega_i, \omega_i, \theta_{collision}$ refers to the Iridium satellite at the time of closest approach, and $a_c, e_c, i_c, \Omega_c, \omega_c$ refers to the Cosmos satellite.

The Iridium satellite carries on-board a hydrazine thruster, whose specifications are listed in Table 2. The mass of the spacecraft is approximated from 586 kg to 500 kg. The predicted miss distance is 0, so it is a direct impact.

$a_i(km)$	7155.8	$a_c(km)$	7155.8
e_i	0	e_c	0
$i_i(deg)$	86.6	$i_c(deg)$	74
$\Omega_i(deg)$	230	$\Omega_c(deg)$	328.29
$\omega_i(deg)$	328	$\omega_c(deg)$	316.25
$\theta_{collision}(deg)$	318.47		

Table 1: Iridium and Cosmos orbital parameters.

Thrust (N)	1
Isp (s)	220
Mass (kg)	500

Table 2: Iridium 33 propulsion parameters.

4.2 IMPULSIVE CAM

In order to compute the optimal impulsive collision avoidance manoeuvre, a maximum Δv of $0.1 \times 10^{-3}\,km\,s^{-1}$ is assumed. In Figures 3 and 4 it is shown the resultant collision probability and the corresponding miss distance; $\Delta\theta$ is the angular distance from the closest approach, and it is expressed in orbits $[2\pi]$. Note that even when the miss distance is 0, the probability is not 1, because of the uncertainty associated to the orbits. The clear favourable manoeuvre points observable in the collision probability plot are due to the relative motion dynamics: since the probability decreases more rapidly in the ξ direction, the manoeuvre should take place in the opposite point in the orbit with respect to the collision [5]. In Figures 5 and 6 the manoeuvres' angles are shown. σ represents the in-plane rotation, opposite to the orbital angular momentum, while γ is the out-of-plane rotation [5]. It is possible to notice that the manoeuvre tends to become more tangential as the anticipation time increases, and that an out-of plane component is usually present. In Figure 7 the b-plane positions after the manoeuvres are shown, together with the error ellipse. The positions tend to follow the semi-minor axis of the ellipse, being it the direction where the collision probability diminishes more quickly.

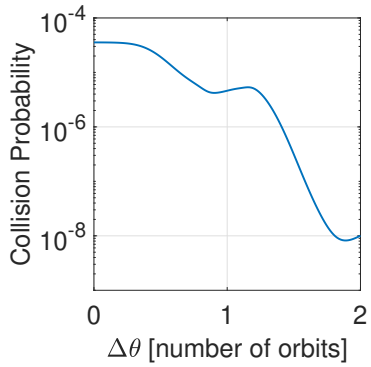

Figure 3: Collision Probability trend of the impulsive manoeuvre.

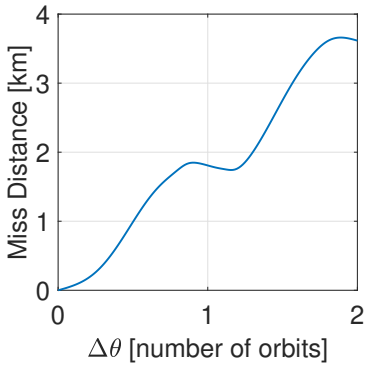

Figure 4: Miss Distance trend of the impulsive manoeuvre.

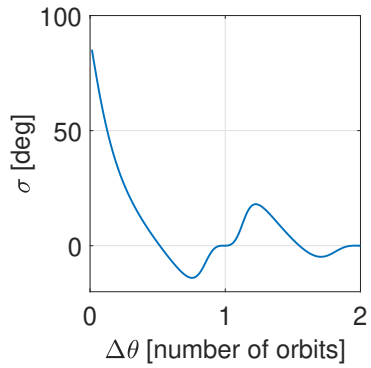

Figure 5: σ trend of the impulsive manoeuvre.

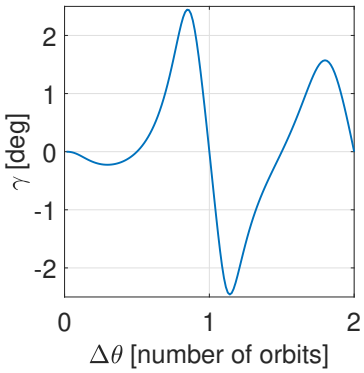

Figure 6: γ trend of the impulsive manoeuvre.

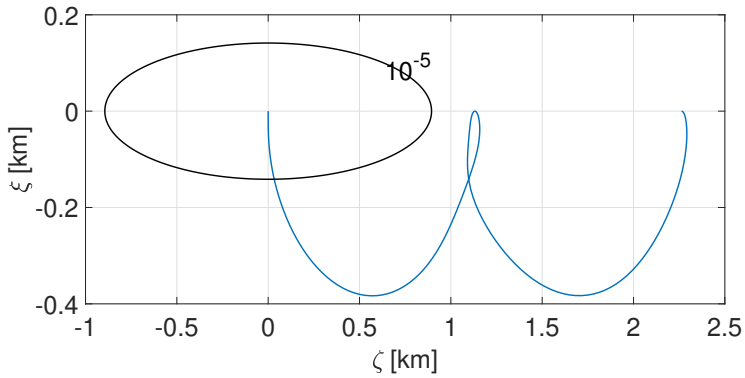

Figure 7: b-plane positions after the impulsive manoeuvres.

4.3 FBC RESULTS

In this section the results relative to the finite-burn conversion illustrated in Section 3.1 are shown.

In order to evaluate the convenience of the conversion to finite-burn, the efficiency η_c is computed as

$$\eta_c = \frac{\|\Delta \boldsymbol{v}_{impulsive}\|}{\|\Delta \boldsymbol{v}_{finite-burn}\|}, \tag{186}$$

where the finite-burn $\Delta \boldsymbol{v}$ is obtained by integrating the control acceleration $\boldsymbol{a}_c$ simultaneously with the equations of motion, once the TPBVP is solved and all the initial conditions to have a well-posed initial value problem are available.

$$\Delta \boldsymbol{v} = \int_{t_i}^{t_f} \boldsymbol{a}_c \, dt = \int_{t_i}^{t_f} \frac{T_{max}}{m} u \boldsymbol{\gamma} dt \,. \tag{187}$$

Therefore, as figures of merit for the conversion, the efficiency and the propellant mass consumed $\Delta m = m_f - m_i$ are chosen. Their mean values are listed in Table 3, and their point values are shown in Figures 8 and 9.

η_c	0.98
$\Delta m(kg)$	0.02

Table 3: Figures of merit of FBC.

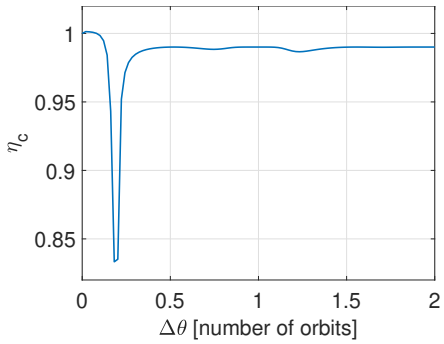

Figure 8: efficiency of FBC.

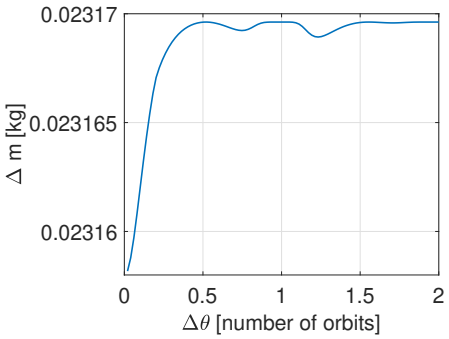

Figure 9: Δm trend of FBC.

From Figure 8 it is possible to see that the efficiency remains constant for all the manoeuvres converted when the impulsive $\Delta\theta$ is higher than ≈ 0.3 orbits. There is then a sudden lost of efficiency and a consequent asymptote to the value $\eta_c = 1$. This behaviour is consistent with the behaviour of the mass in Figure 9, and it is easily explained looking at Figure 3: the collision probability resulting from the optimal impulsive manoeuvre tends to increase exponentially as the collision becomes closer, and reaches the nominal value as $\Delta\theta \to 0$. For $\Delta\theta < 0.3$ orbits the time available is no more sufficient for an optimal conversion, consequently there is a sudden loss of efficiency. Near the collision the constraints on the final distance relaxes, and the miss distance tends to 0, therefore time of flight available becomes more than enough to satisfy the boundary conditions (as it is possible to see in Figure 12), and as the efficiency tends to unity, the propellant needed diminishes.

In order to obtain the discontinuous control law, the exponential function (75) is chosen to perform the continuation on u; the parameter p has been increased first with 5 iterations where $p_{k+1} = p_k + 2$ and then with other 5 iterations with $p_{k+1} = p_k + 20$, starting from a value of $p_1 = 1$.

From Figures 10-12 it is possible to see that for manoeuvres converted far from the collision, the thrust is mainly tangential, while for manoeuvres close to the collision, both a radial and an out-of-plane component (not visible in the plots) start to arise, emulating then the behaviour of the impulsive manoeuvre. The switching function, the thrust ratio and the thrust components are plotted as function of the burn time, computed with (96).

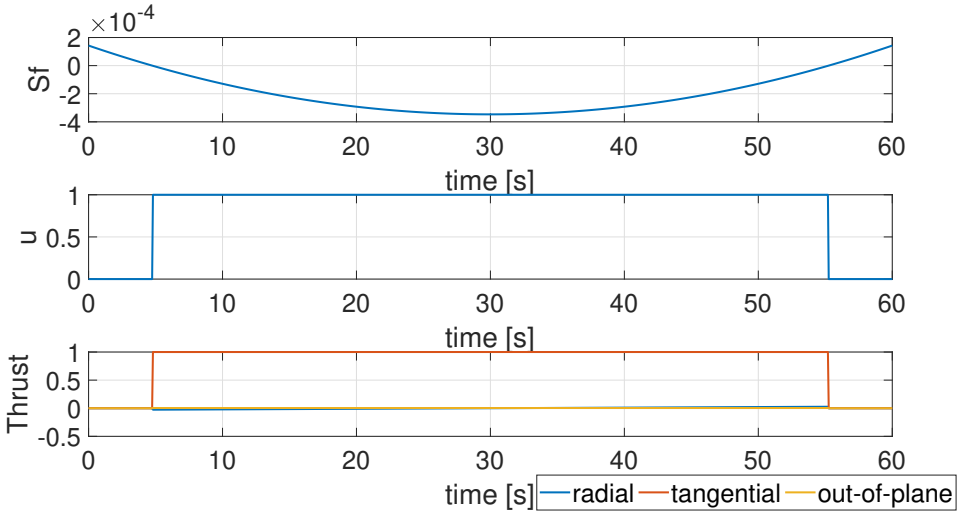

Figure 10: FBC switching function, thrust ratio and components at $\Delta\theta_{imp} = 1$ orbits.

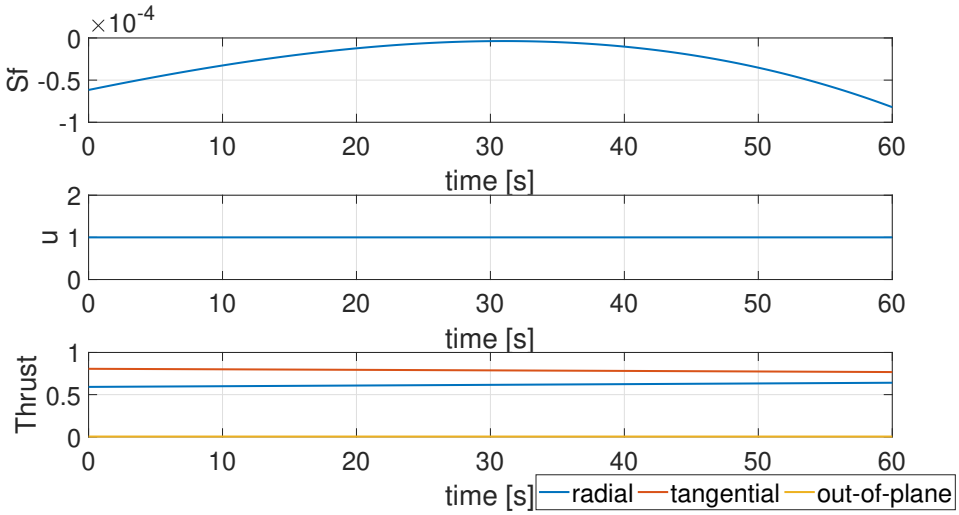

Figure 11: FBC switching function, thrust ratio and components at $\Delta\theta_{imp} = 0.16$ orbits.

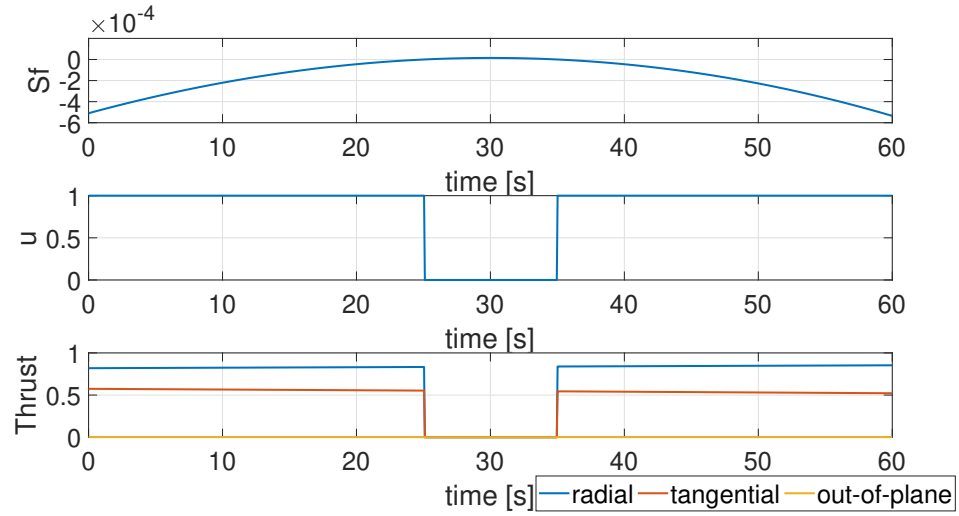

Figure 12: FBC switching function, thrust ratio and components at $\Delta\theta_{imp} = 0.12$ orbits.

4.4 FOP RESULTS

In this section the results of the application of FOP (see Section 3.3) are shown.

Figure 13 reports the P_c profile obtained with the application of the minimum-fuel formulation for the collision probability minimization problem explained in Section 3.3. It is possible to see the profiles corresponding to the application of three different weights W on the terminal cost. The flat behaviour particularly evident for $W = 1$ is due to the trade off between the terminal cost and the path cost illustrated in Section 3.2.2: close to the collision, the mass expenditure is considered too high with respect to the achievable P_c and the resulting control law corresponds to no thrust, therefore P_c assumes the nominal value $P_{cn} = 3.775 \times 10^{-5}$. The application of higher weights yields an higher mass expenditure and a lower P_c, therefore it is possible to obtain $P_c < P_{cn}$. As for EOP, more than one solution exists for the same initial manoeuvre point. Because of the high computational time required by FOP to converge to the optimal solution, the random search performed for EOP (see next section) is not applicable to this method. Nevertheless, the presence of more than one solution resulted evident from the outcomes of the simulations if the ACT is adopted for each $\Delta\theta$: the algorithm converged to values of Pc of differing orders of magnitude one from the other, causing evident jumps in the Pc profile. In order to converge to the same branch of solutions, every iteration is made dependant from the previous one: the costate solution found at the initial manoeuvre point $\Delta\theta_n$ is used as initial guess for the manoeuvre point $\Delta\theta_{n+1}$, with $\Delta\theta_n > \Delta\theta_{n+1}$.

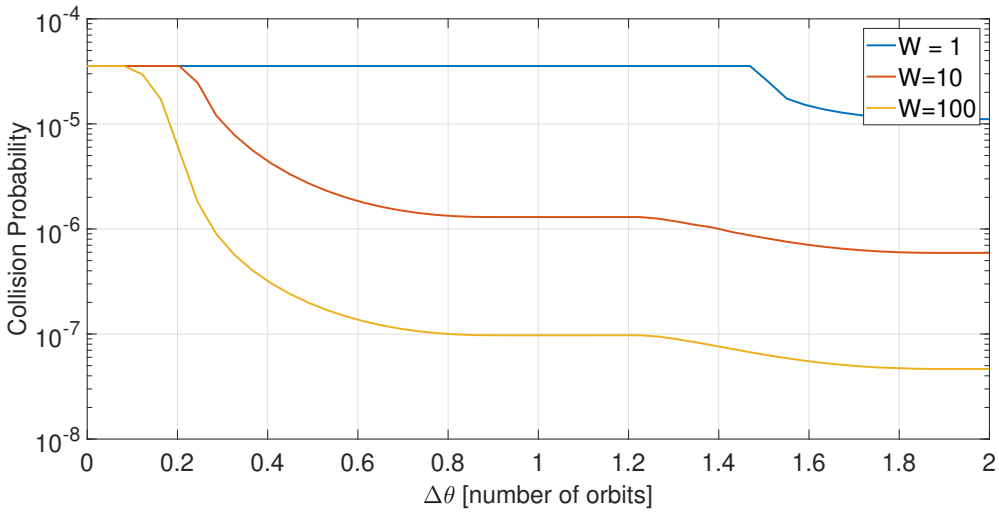

Figure 13: Collision Probability trend of FOP.

In Figure 14 the b-plane positions corresponding to the probability profiles with two different weights are shown.

These results are consistent with the ones of the optimal impulsive CAM (Section 2.4): the final positions, as $\Delta\theta$ diminishes, tend to be aligned with the semi-minor axes of the error ellipse, since it is the direction where the collision probability diminishes more rapidly. For angular distances larger than $\Delta\theta = 1$ orbit, the pattern appears to repeat, on a different scale. The presence of different solutions can be perceived looking at the distribution of the solutions around the ellipse: they are split among two main patterns, as it is more visible in the analysis shown in

Sections 4.5 and 4.7. These patterns differ very little in terms of achieved collision probability, therefore FOP converges alternatively to both of them. One pattern is visible for manoeuvres performed up to one orbit in advance with respect to the collision, the other pattern is the first pattern reflected with respect to both semi axes. In fact, for manoeuvres performed from one to two orbits in advance, it is possible to see the presence of solutions on both sides of the plot. This behaviour is better investigated in Sections 4.5 and 4.7.

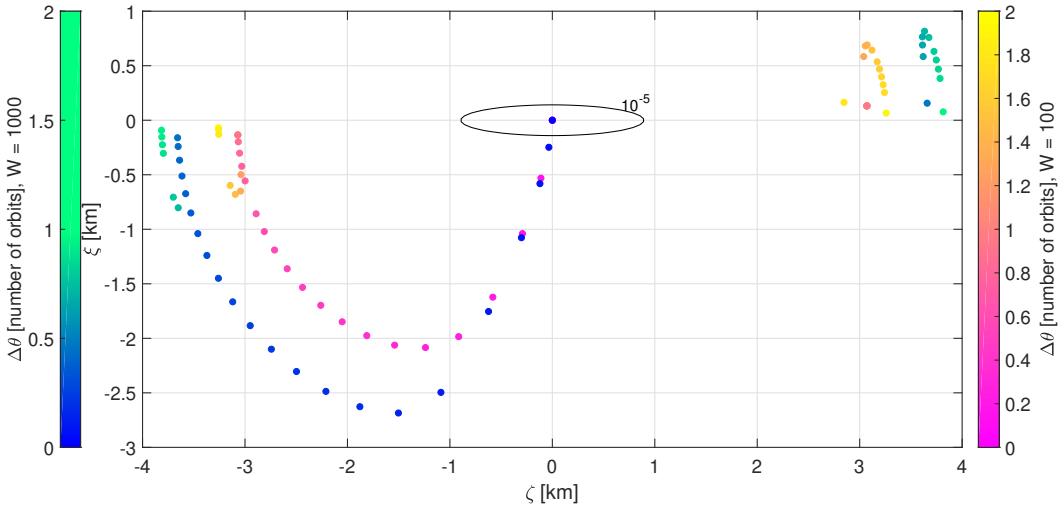

Figure 14: b-plane positions of FOP.

In Figure 15 it is shown the propellant mass behaviour. When the manoeuvre starts far from the collision point, lower P_cs are achieved with lower Δm. The flat part of the plots corresponds to the flat part of P_c in Figure 15: when no thrust is applied, Δm is obviously zero.

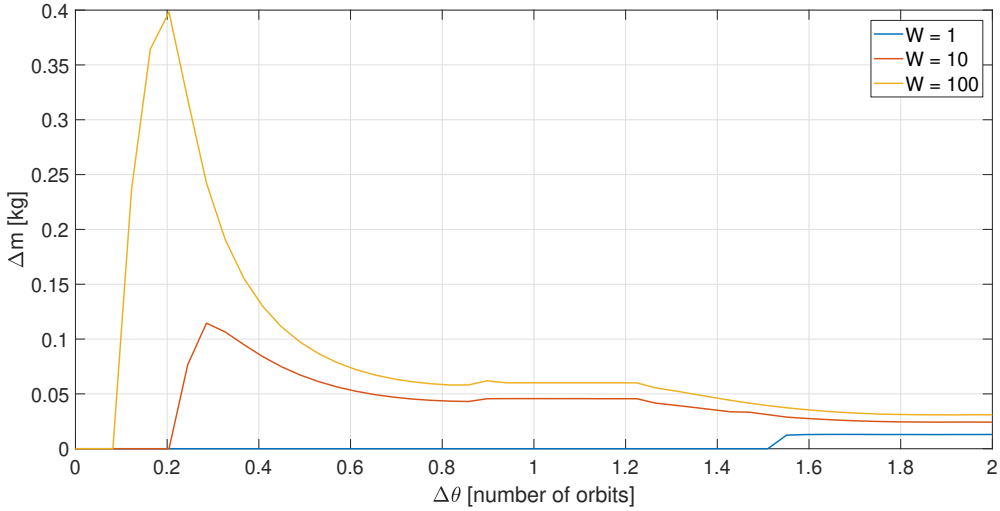

Figure 15: Δm trend of FOP.

In Figures 16 and 17 it is shown the typical bang-bang optimal thrust profile for manoeuvres starting 2 orbits prior to collision and half orbit prior to collision,

respectively. Thrust components are plotted as function of the time to collision tc. Consistently with the literature [14], the thrust usually has an out-of-plane and radial component. When the distance from the collision grows, the thrust becomes mainly tangential. When the thruster is on, the thrust magnitude is equal to 1N.

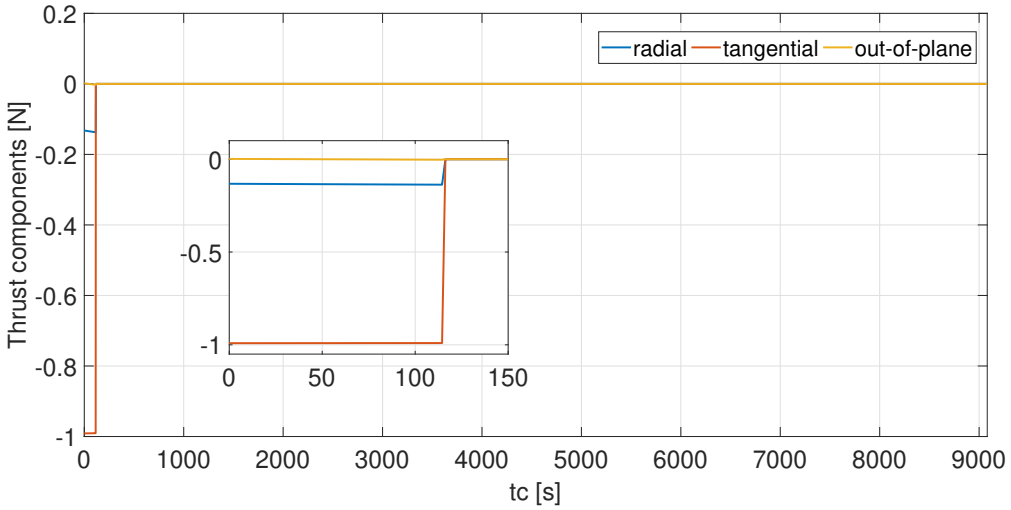

Figure 16: FOP thrust components at $\Delta\theta = 1.5$ orbits, achieved $P_c = 6 \cdot 10^{-9}$, $W = 1000$.

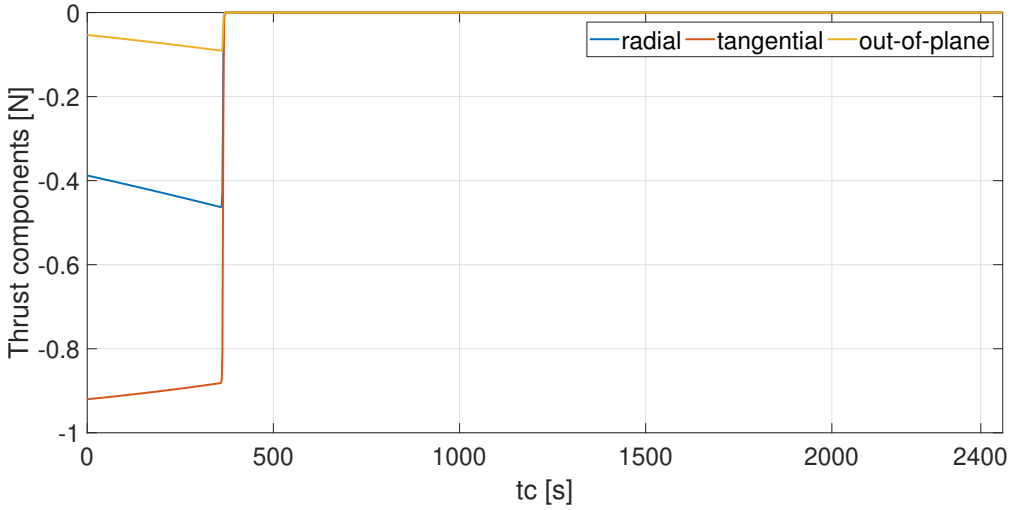

Figure 17: FOP thrust components at $\Delta\theta = 0.5$ orbits, achieved $P_c = 3 \cdot 10^{-8}$, $W = 1000$.

The optimal discontinuous solution is obtained with the continuation method already explained in Section 75, using the exponential function. Looking at the boundary conditions (117), it is possible to see that a trivial solution corresponding to $\lambda(t) = 0$ exists. Low thrust magnitudes correspond to low costates magnitudes. When the manoeuvre starts more than one orbit in advance with respect to the collision, the needed thrust is particularly low, therefore costates are nearly zero. This implies that a very slow continuation has to be performed, since abruptly changes in the continuation parameter p reflect in convergence issues, yielding the trivial solution.

It is found that a continuation on the parameter p of the kind showed in Figure 18 works for almost all the manoeuvres points up to three orbits in advance with respect to the collision.

```
set p to one
set counter to one

while counter is less or equal to five

    add one to p

end while

 set counter to one

 while counter is less or equal to ten

    add five to p

 end while

 set counter to one

 while counter is less or equal to fifteen

    increment p of 150%

 end while
```

Figure 18: FOP continuation method, pseudocode.

4.5 EOP RESULTS

In this section the results of the application of the minimum energy formulation explained in Section 3.4 are illustrated.

In order to have a preliminary idea of the possible solutions, an initial random search is initialized. Since the problem is normalized, the search space for each costate is restricted to $\lambda \in (0, 1]$. The 0 is excluded from the acceptable solutions since, looking at (146), it is possible to see that the solution $\lambda(t_f) = 0$ satisfies the terminal boundary conditions when $\mathbf{r}_f = \mathbf{r}_c$, that is when there is no deviation from the nominal trajectory. As a consequence, an initial condition of $\lambda(t_i) = 0$ leads to the trivial solution of no thrust.

The search is made with 100 costates per manoeuvre point, and the results are shown in Figure 19. For manoeuvre points $\Delta\theta < 0.5$ orbits there are two main solution branches, that then divide in 2 sub-branches. For $\Delta\theta > 0.5$ orbits only the branch corresponding to lower P_cs is found. From now on, the branch correspondent to higher P_cs is going to be called branch 1, and the other branch 2. In order to follow one of the two main branches, the ACT 3.3.1 is again used to find first guesses for the Newton's method. To avoid discontinuities and jumps between the two branches, the solution found for an initial manoeuvre point $\Delta\theta_n$, is used

as first guess for the initial manoeuvre point $\Delta\theta_{n+1}$. In Figure 20 the positions corresponding to each solution are shown. Both the solutions corresponding to the applied weights $W = 1$ and $W = 100$ are illustrated: it is possible to notice that, the higher the weight, the more the positions shifts along the ellipse semi-axes. Positions corresponding to the branches labelled 1 and 3 shifts vertically along the semi-minor axis, while positions labelled 2 and 4 shifts horizontally along the semi-major axis.

The vertical branches (1 and 3), correspond to branch 2 solutions. This is a trivial result, since along the semi-minor axis the collision probability diminishes more quickly. This behaviour will be further examined in Section 4.7, since the smaller computational time of the Semi-Analytical Method enables to perform more detailed analysis.

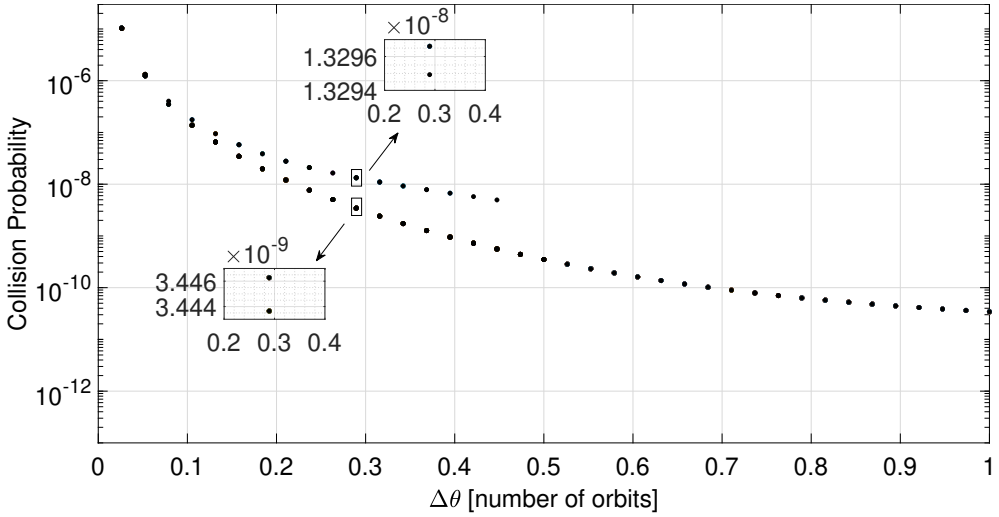

Figure 19: Collision Probability trend resulting from the EOP random search.

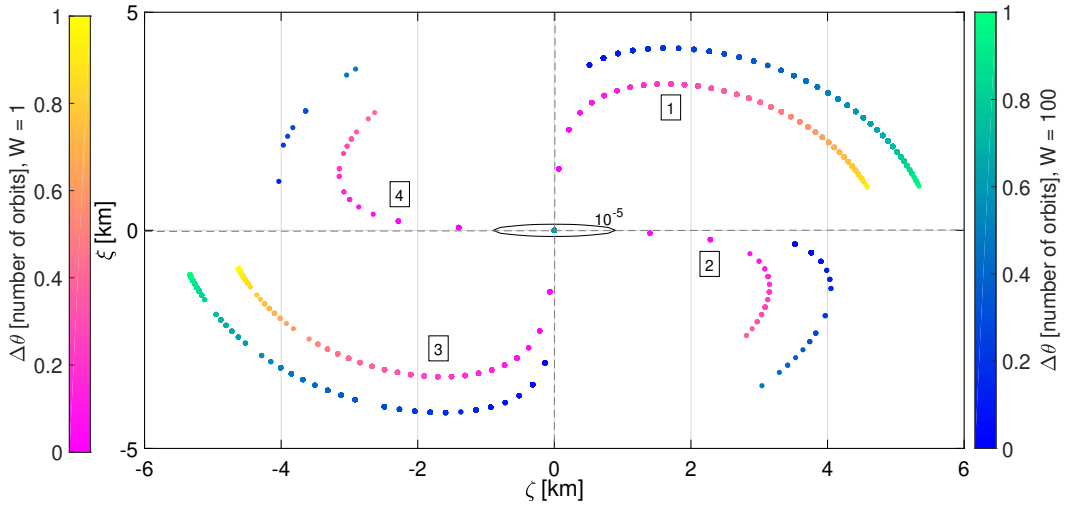

Figure 20: b-plane positions resulting from the EOP random search.

In Figure 21 the collision probability trend resulting from the energy-optimal problem illustrated in Section 3.4 is shown. Three different weights are applied to

the terminal cost P_c in the cost function, in order to obtain different probability curves; in so doing, it is possible to choose the solution that matches the desired threshold. Furthermore, the solution is found to be highly dependent on the guess for the initial costates: it oscillates between the various solutions found in the random search and illustrated in Figure 19. In order to have a continuous probability profile, the iterations are made co-dependant: the solution for the initial costates found for the manoeuvre starting at $\Delta\theta_n$ is used as initial guess for the manoeuvre starting at $\Delta\theta_{n+1}$. The use of the ACT (Section 3.3.1) to compute the initial guesses yields the solution to converge to the lower P_c branch. In Figure 22 the b-plane positions corresponding to $W = 1$ are shown. The flat part of the collision probability plot for $W = 1$ is due to the fact that the trade off between collision probability (terminal cost) and the energy cost (integral cost) yields to the no-thrust solution, therefore the collision at the closest approach remains the nominal one, $P = 3.775 \times 10^{-5}$.

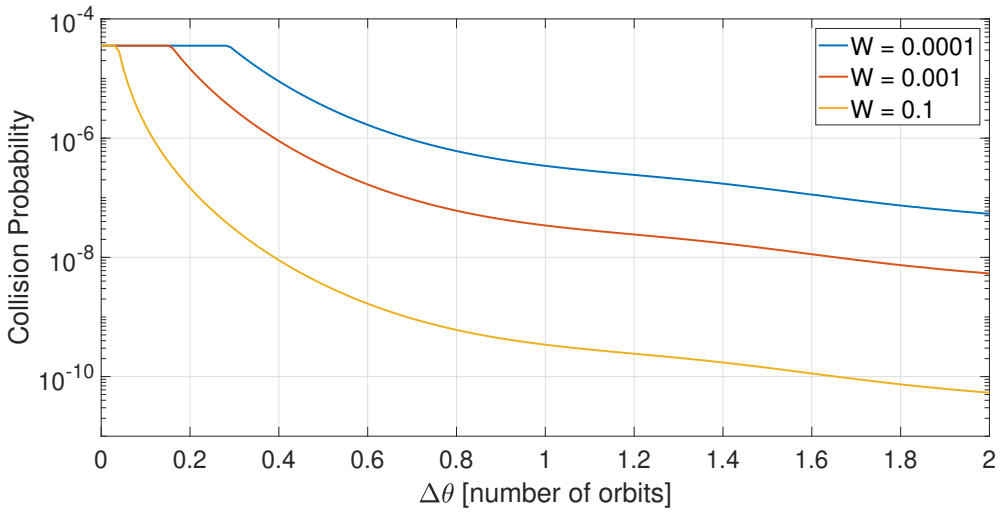

Figure 21: Collision Probability trend of EOP.

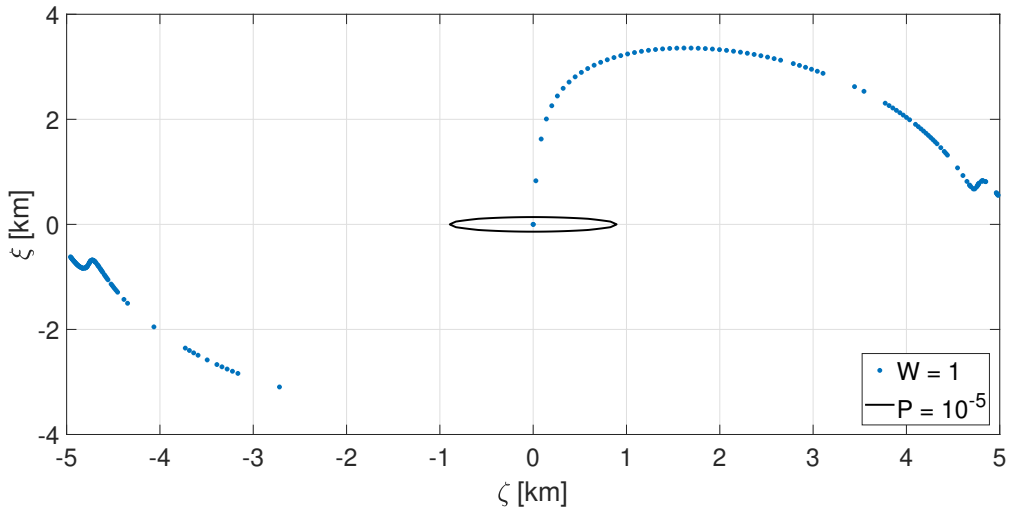

Figure 22: b-plane positions of EOP when W = 1, initial guesses estimated with ACT.

In Figure 23 the $\Delta m = m_f - m_i$ associated to each manoeuvre point is shown. It decreases as the distance from the predicted impact increases. In conclusion, the farer the manoeuvre starts, the more efficient it is, both in terms of propellant, and achieved collision probability.

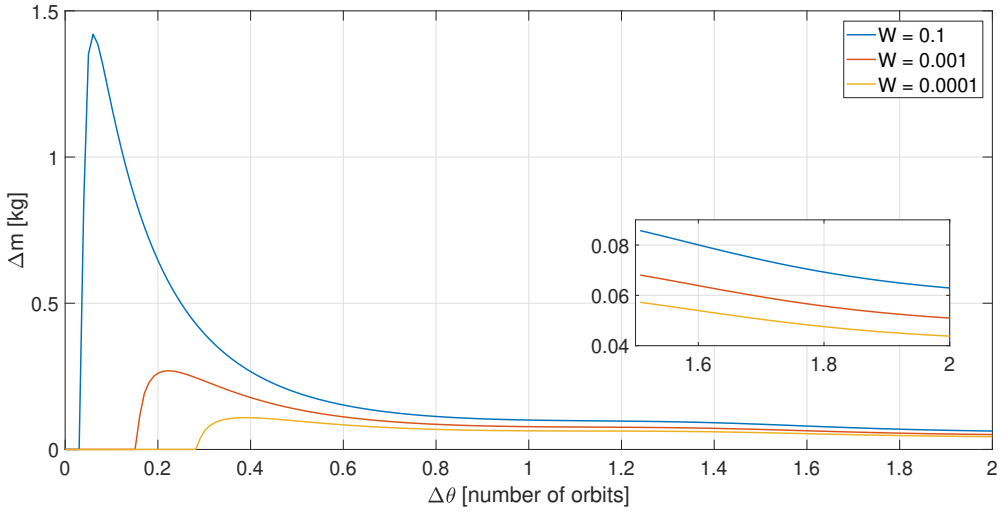

Figure 23: Δm trend of EOP.

The continuous thrust profiles showed in Figures 24 and 25 reflect the behaviour already noticed in FOP and FBC thrust profiles: when the distance from the collision grows, the thrust becomes mainly tangential, while close to the collision an out-of-plane and radial components are present. In fact, when $\Delta\theta = 2$ orbits, the thrust magnitude and the tangential component almost overlap, while for $\Delta\theta = 0.5$ orbits the radial and out-of-plane components assume values comparable with the tangential one.

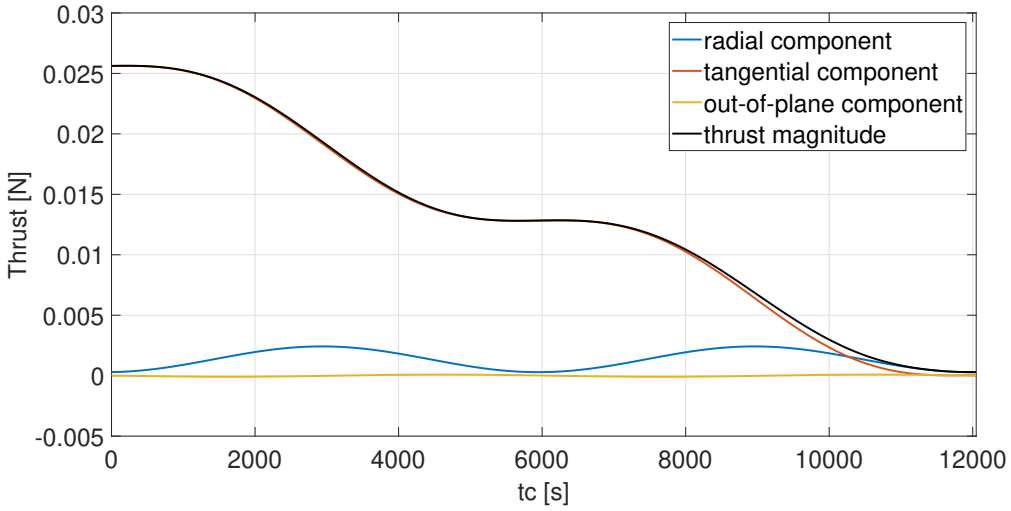

Figure 24: EOP thrust profile at $\Delta\theta = 2$ orbits, achieved $P_c = 5 \cdot 10^{-12}$, $W = 1$.

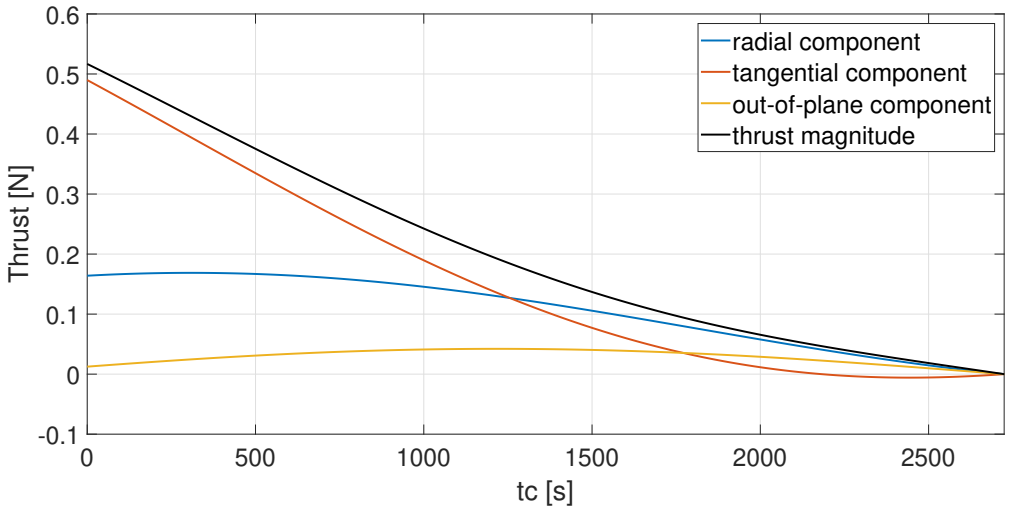

Figure 25: EOP thrust profile at $\Delta\theta = 0.5$ orbits, achieved $P_c = 5 \cdot 10^{-10}$, $W = 1$.

4.6 AM RESULTS

In this section the results of the analytical approach developed in Section 3.5 are presented. Figure 26 shows the collision probability profile as function of ϵ_{AM}. Greater values of ϵ_{AM} yield lower values of P_c, since the distance from the nominal trajectory increases. This is the only method developed in this dissertation where it is possible to choose the desired P_c in advance, and then compute the control law.

The direction d_{max} where the final position of the spacecraft $\mathbf{r}_f$ is imposed to be is computed in Section 3.5, and it is shown in Figure 29; as predictable, it follows the semi-minor axis of the error ellipse. Figure 27 shows the mass profile. The constant probability curves are plotted as function of the manoeuvre starting point: it is possible to notice a minima at one orbit in advance, followed by local minima at multiples of one orbit. The mass consumption does not decreases with $\Delta\theta$.

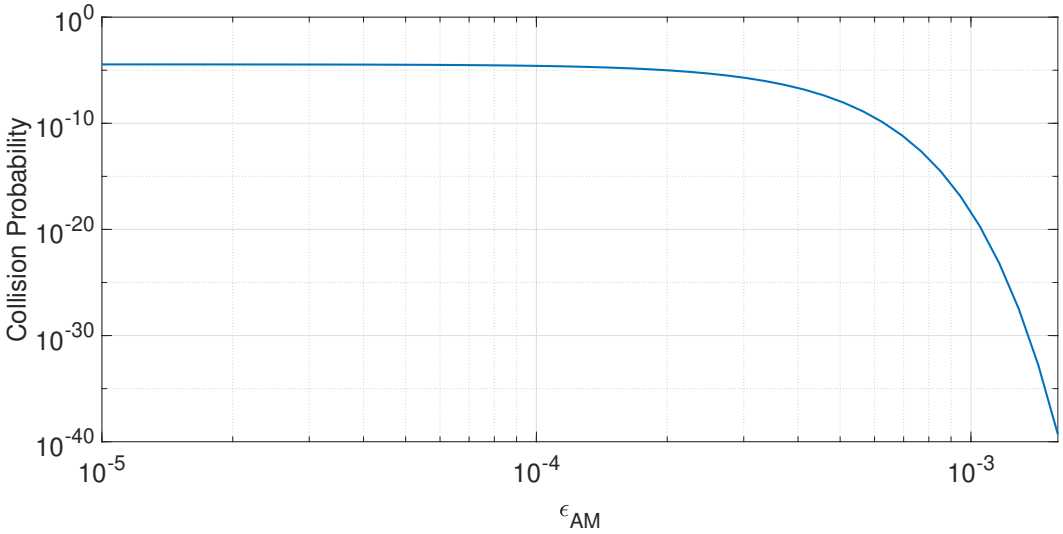

Figure 26: Collision Probability trend of AM.

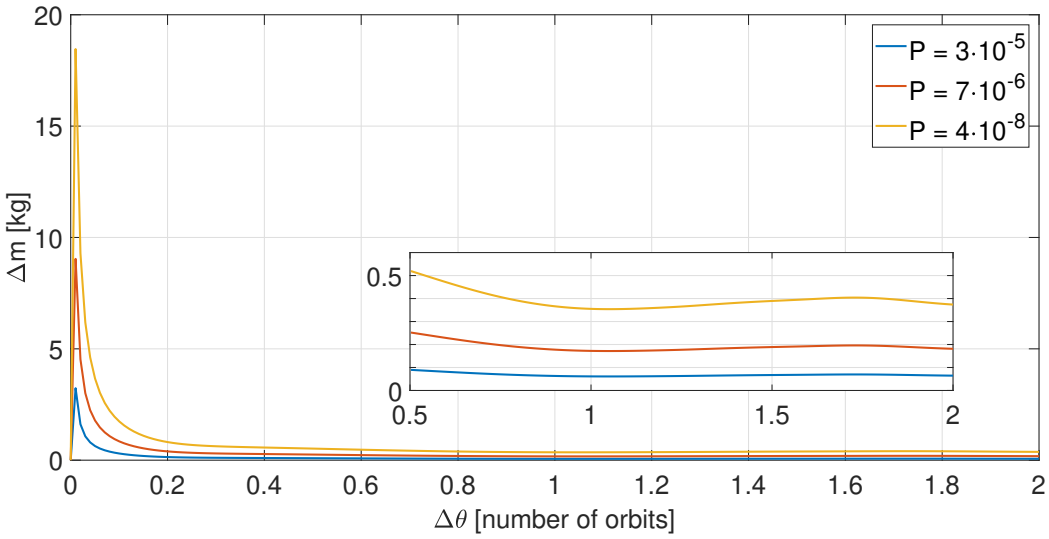

Figure 27: Δm trend of AM.

4.7 SAM RESULTS

In this section the results of the semi-analytical approach developed in Section 3.6 are reported. As it was already done for the EOP, in order to obtain a complete picture of the possible solutions, a set of random initial guesses per manoeuvre point to solve equations (184) is used.

Every set of guesses is created randomly by varying the nominal initial guess $\delta\mathbf{r}_0 = \mathbf{d}_{max}$ in the neighbourhood bounded by a and b, chosen as

$$a = \delta\mathbf{r}_0 - 5\delta\mathbf{r}_0\,, \tag{188}$$

$$b = \delta\mathbf{r}_0 + 5\delta\mathbf{r}_0\,. \tag{189}$$

The solution is found through Newton's iterations, and the algorithm converged for all the initial guesses. The results can be seen in Figure 28. Consistently with the fact that this formulation is the linearisation of the EOP, the solutions found agree with the ones of the minimum-energy formulation, with the exception of the initial discontinuity in the SAM curve, that is better visible in Figure 34, where the collision probability profiles of SAM and EOP are compared. In Figure 29, the b-plane positions for $W = 1, 100, 10^4$ are shown. The positions plotted correspond to manoeuvres performed at distances to collision ranging from $\Delta\theta = 0$ to $\Delta\theta = 1$ orbit. Lighter colours correspond to higher distances to collision.

Comparing EOP and SAM results it is found that the error introduced by the linearisation is of the order of meters. The comparison between these two methods is better illustrated at the end of this section. Unlike EOP, this time the two main probability branches are found for all the manoeuvre points.

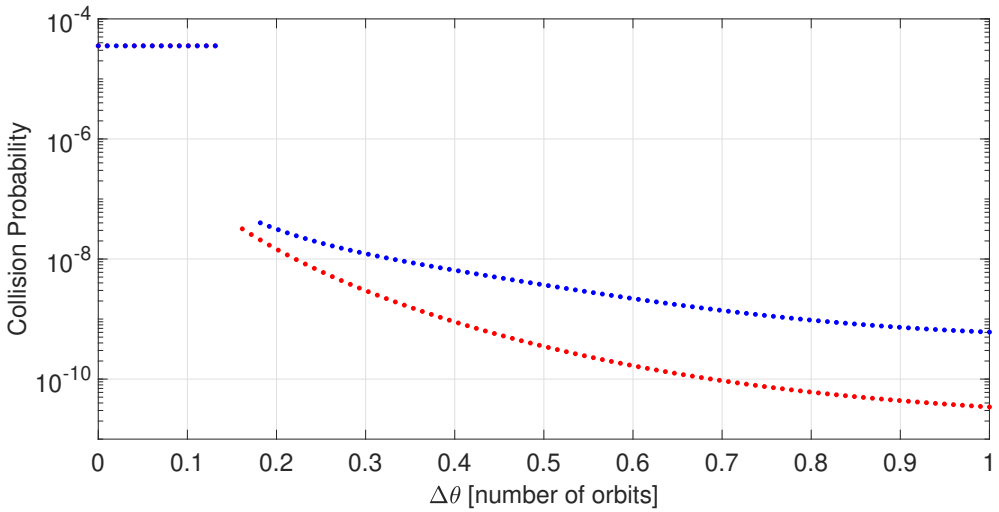

Figure 28: Collision Probability trend of the SAM random search with W = 1.

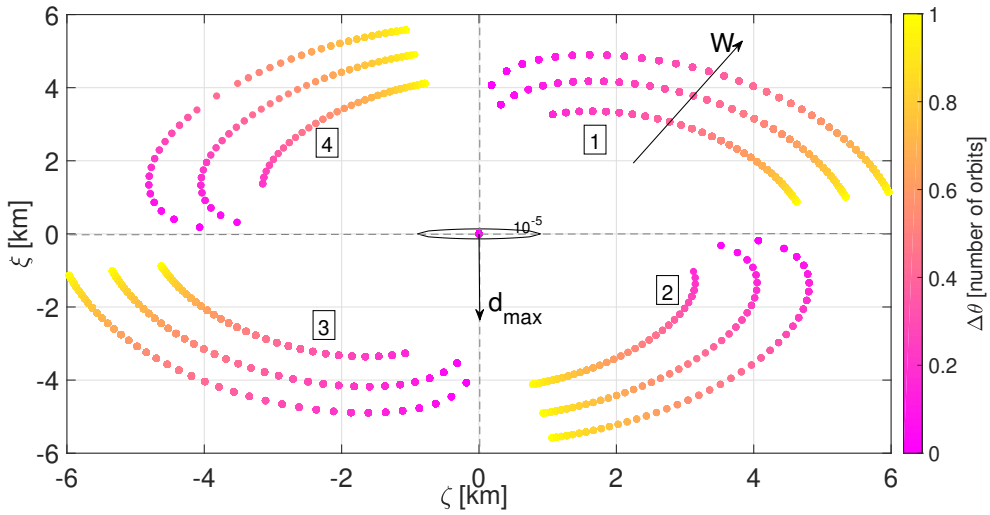

Figure 29: b-plane positions of the SAM random search.

The mass and miss distance profiles corresponding to the two solution branches are visible in Figures 30 and 31. The curve corresponding to the probability branch 2 (the red one) is the one corresponding to lower masses: in fact, the positions of branch 2 are closer to the semi-minor axis of the ellipse (branches 1 and 3 in Figure 29), therefore the probability diminishes more quickly, and it is possible to obtain lower P_c with less mass consumption. It is interesting to notice that the horizontal position branches (labelled 2 and 3) correspond to smaller deviations from the nominal trajectory, that is smaller miss distances, but to higher mass consumption. Therefore, the red branches in Figures 28, 30 and 31 are solutions that grants the minimum P_c with the least mass consumption (the vertical positions branches), while the blue branches correspond to higher P_c and Δm, but lower miss distance.

In Figure 32 it is visible the collision probability profile as function of W. As it was already done for the FOP/EOP, in order to avoid jumps between the different branches, the result of each iteration is used as initial guess for the next one.

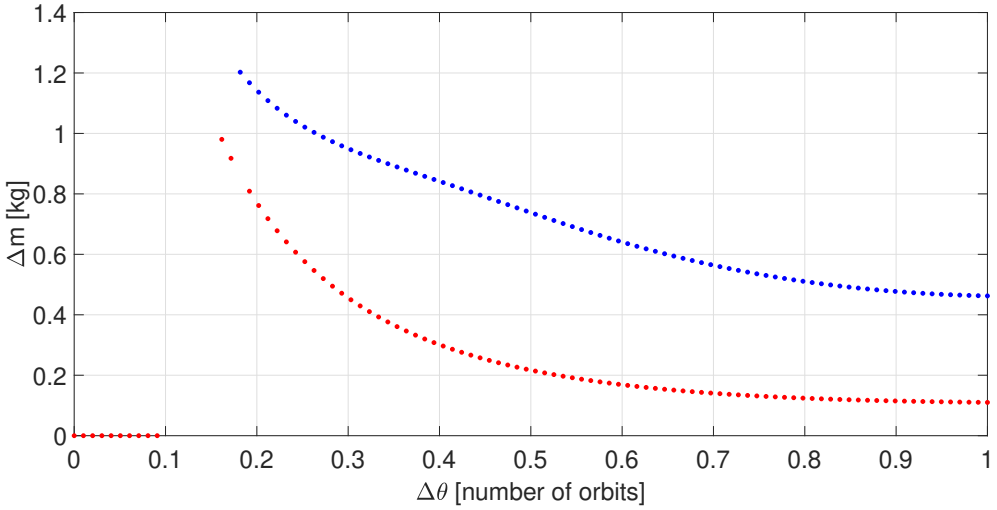

Figure 30: Δm trend of SAM, random search with W = 1.

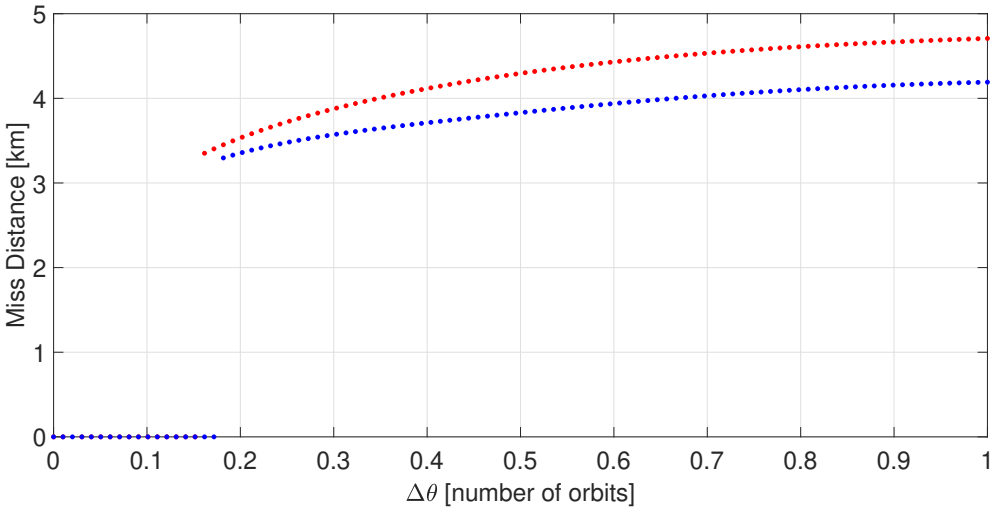

Figure 31: Miss Distance trend of SAM, random search with W = 1.

Furthermore, the first iteration is chosen to be the one closer to the collision, since the smaller the deviation from the nominal trajectory, the more accurate the linearised solution is. The choice of the closer point to collision as first iteration point yields problems when the weight is particularly small, since all the successive iterations tend to converge to the zero-thrust solution. To avoid this problem, the initial guess for iterations with low W is chosen to be the solution belonging to an higher weight branch, for the same $\Delta\theta$. The format of this plots is the same as EOP/FOP one: to different weights correspond different probability profiles. In Figure 33 the mass consumption corresponding to the probability curves is shown.

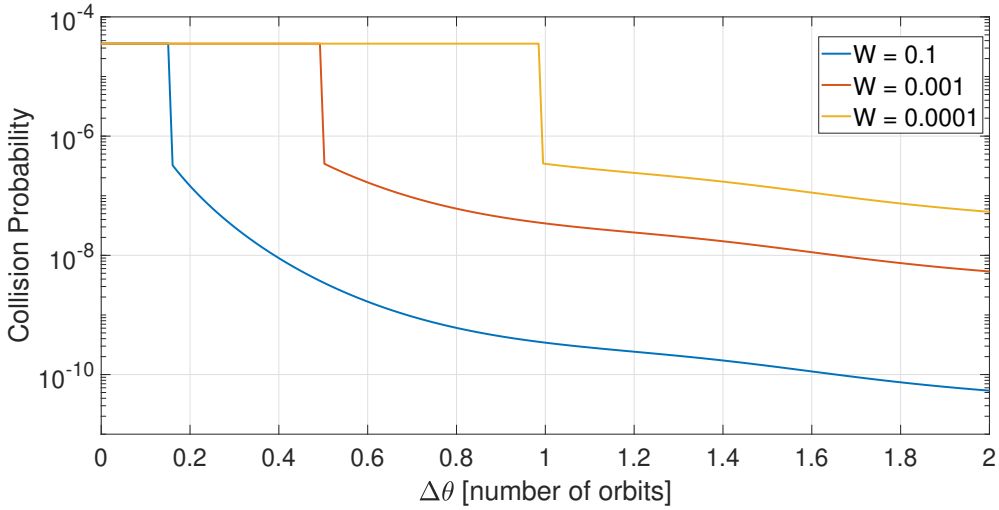

Figure 32: Collision Probability trend of SAM.

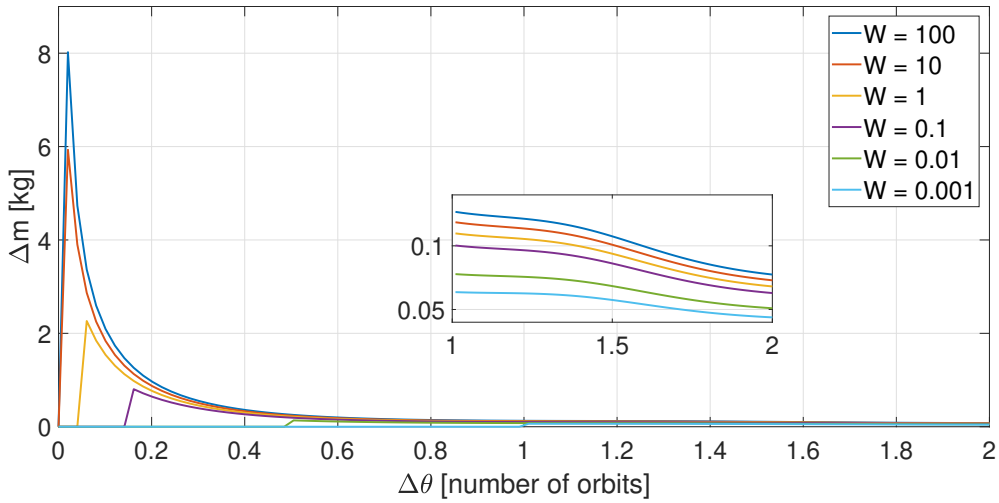

Figure 33: Δm trend of SAM.

In Figures 34 and 35 the probability and mass profiles of EOP and SAM are compared. After a transient dependant on W, the probability curves overlap, and the mass profiles differ on the order of 10^{-4}kg. The weight W has the same value for both the methods. The lower W, the longest the transient, as it is possible to see by comparing Figures 32 and 21, where the P_c of SAM and EOP are shown.

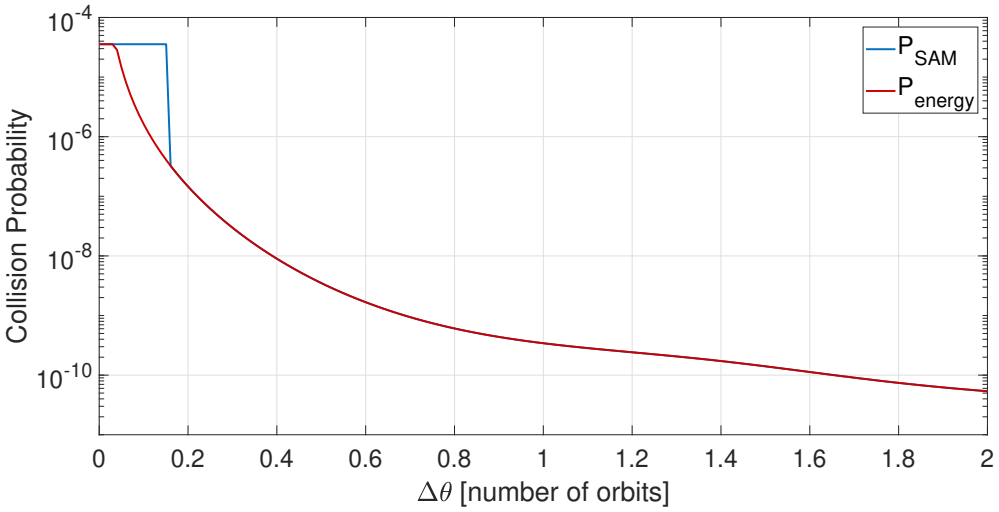

Figure 34: Collision Probability comparison between EOP and SAM with W = 0.1.

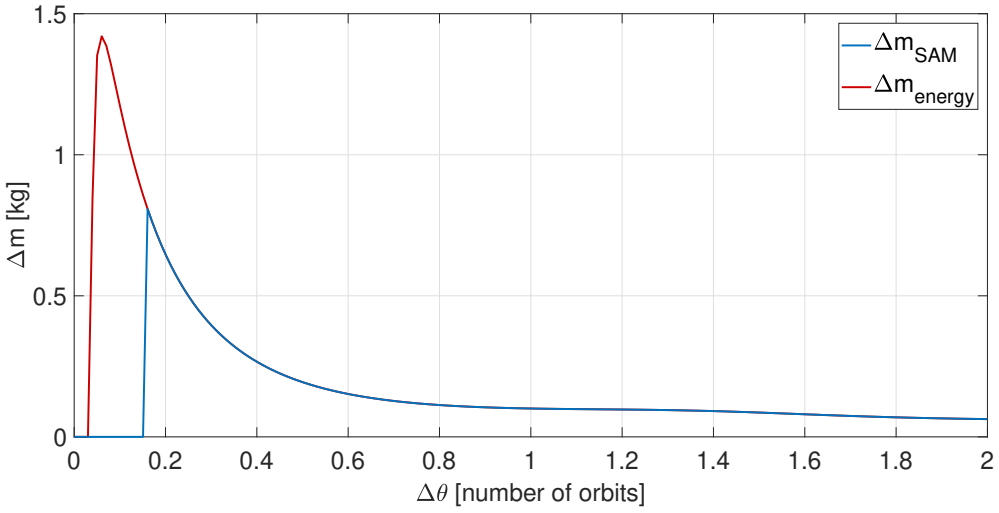

Figure 35: Δm comparison between EOP and SAM with W = 0.1.

4.8 COMPARISONS

In this section the various approaches are compared in terms of mass consumption, computational cost and robustness.

4.8.1 *Mass*

In this section the approaches are compared in terms of mass consumption. In Figure 36 the mass consumptions of AM and SAM are compared, as function of the manoeuvre point, at fixed P_c. At every $\Delta\theta$, the achieved collision probability is the same for both methods.

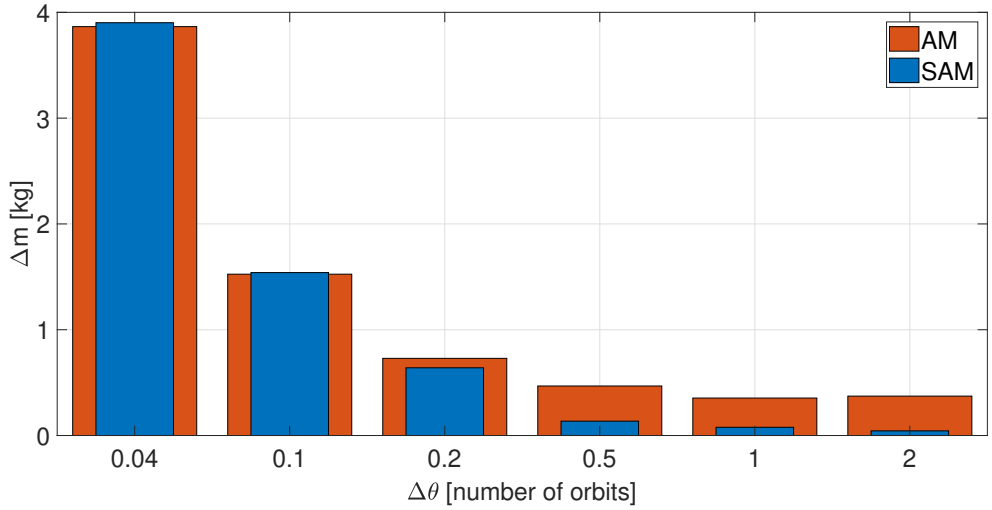

Figure 36: Δm comparison between AM and SAM with W = 0.1.

For manoeuvres performed very close to the collision, AM is more efficient than SAM and, therefore, EOP. In both these approaches, mass consumption is not explicitly inserted as an optimizable parameter; EOP/SAM minimize energy and collision probability, while AM minimize energy and, indirectly, mass and collision probability, since in the analytical method the energy-optimal dynamics is exploited for a transfer to a fixed state situated along the maximum change of P_c at the time of closest approach. For more distant manoeuvres, AM mass oscillatory behaviour definitely affect the performances, and SAM/EOP are more efficient. In Figure 37 it is shown the mass consumption as function of the orbital position, for fixed P_c, of all the approaches. From this plot it is not possible to infer conclusions about the behaviour of the single methods as function of the manoeuvre point, since at every $\Delta\theta$ the collision probability used for the comparison is different. For example, the P_c achieved at $\Delta\theta = 0.6$ orbits is lower than the one achieved at $\Delta\theta = 0.3$ orbits, and AM consumes more mass to achieve a lower collision probability, even if the manoeuvre starts earlier. Apart from AM, the behaviour of the other methods is confirmed by the specific analyses performed in the dedicated sections: the mass consumption decreases with the distance from the collision. The fuel-optimal formulations are, as expected, always the most efficient ones. FBC proved to be always more efficient than FOP but close to the collision, since even for high P_c, FBC mass consumption does not change. The gap between FOP/FBC

and EOP/SAM is minimal compared to the difference with AM, especially when $\Delta\theta$ grows.

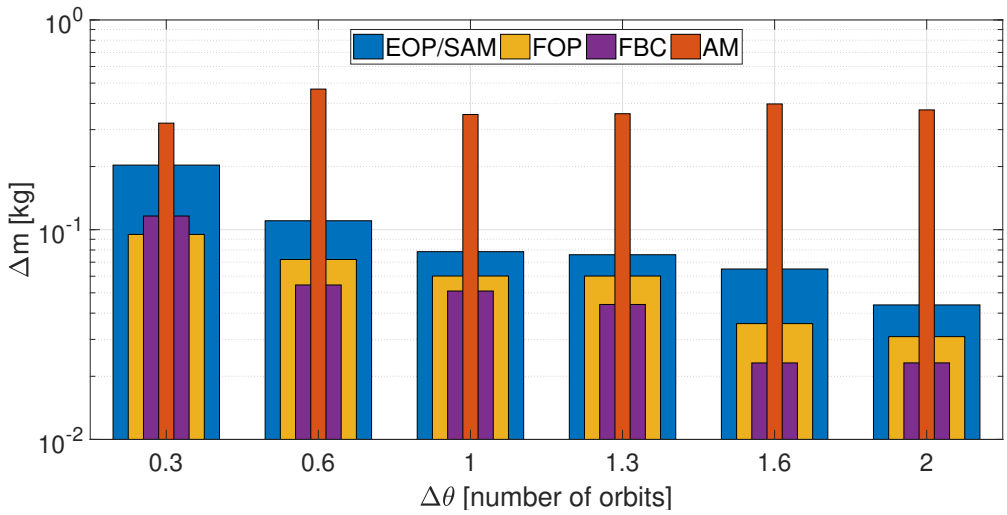

Figure 37: Complete Δm comparison.

4.8.2 *computational time*

In this section the approaches are compared in terms of Computational Time (CT). In Figure 38 CT is plotted as function of $\Delta\theta$. FOP and FBC show a constant behaviour, while CT of EOP, SAM and AM decreases with the decreasing of the time to collision, which is a reasonable behaviour since the methods are mainly based on integrations over tc.

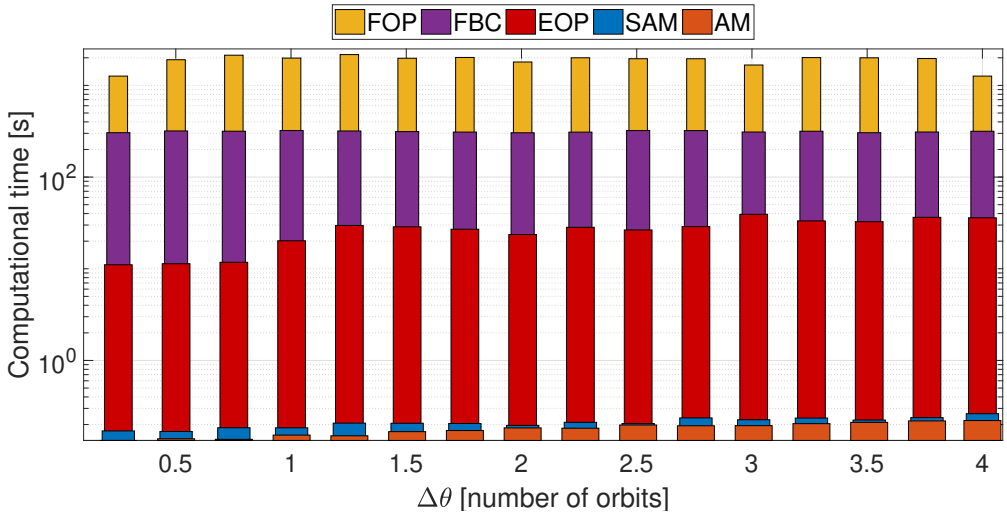

Figure 38: Complete computational time comparison.

In Figure 39 it is shown the comparison between SAM and AM. Because the CT of both methods is of the order of fractions of second, in order to have results independent on the specific simulation conditions, every simulation is repeated 100 times and then averaged. As predicted, the analytical method is always faster than the semi-analytical one.

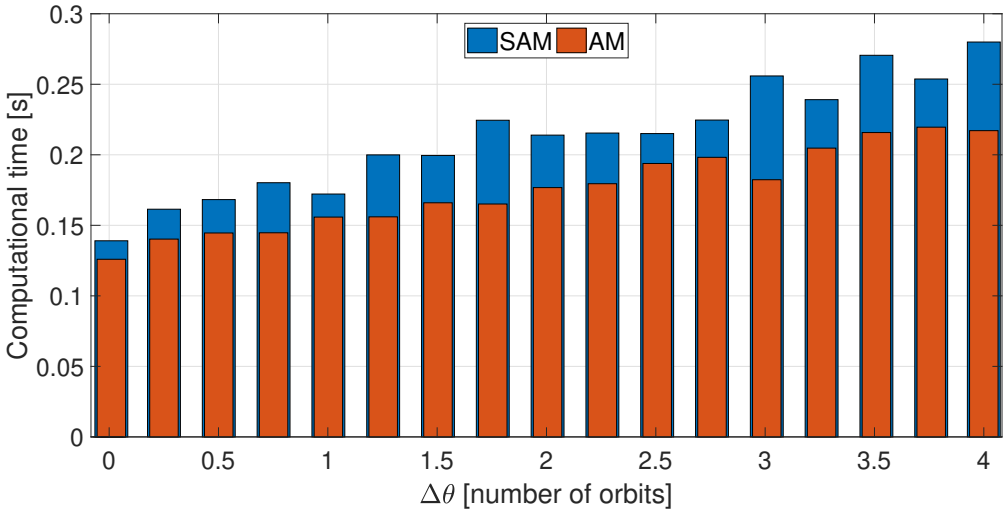

Figure 39: Computational time comparison between AM and SAM.

4.8.3 *Convergence*

In this section the robustness of the numerical and semi-analytical methods is compared and discussed. Figure 40 shows the percentage of converge of the EOP random search. Far from the collision, less thrust is needed to achieve the same collision probability, therefore the costates magnitude is significantly lower than unity, while the opposite happens for manoeuvres performed close to the collision point. These considerations reflect in the behaviour of the convergence percentage: when the initial guesses' magnitude is $|\lambda_0| = 1$, the convergence percentage increase as $\Delta\theta$ decreases, while the opposite happens for $|\lambda_0| = 1e^{-5}$.

Table 4 shows when FOP and EOP converges if the ACT is used to guess the initial costates, as function of $\Delta\theta$. Regarding EOP, the algorithm was not able to reach the desired tolerances, set at 10^{-10}, with less than 800 iterations, for manoeuvres performed at 2 orbits $< \Delta\theta <$ 3 orbits. FOP is less sensitive to initial guesses but it is sensitive to the continuation rate, as it was already mentioned in FOP dedicated section.

FBC does not show convergence issues, and it is definitely less sensitive to the continuation method: since the mass consumption is constant, as well as the burn-time, the continuation rate is not dependant on the manoeuvre point, and the impulsive Δv angles proved to be an optimal initial guess for the velocity costate.

The robustness of SAM is tested with the set of initial guesses described in (189). It converged for the entire set of guesses.

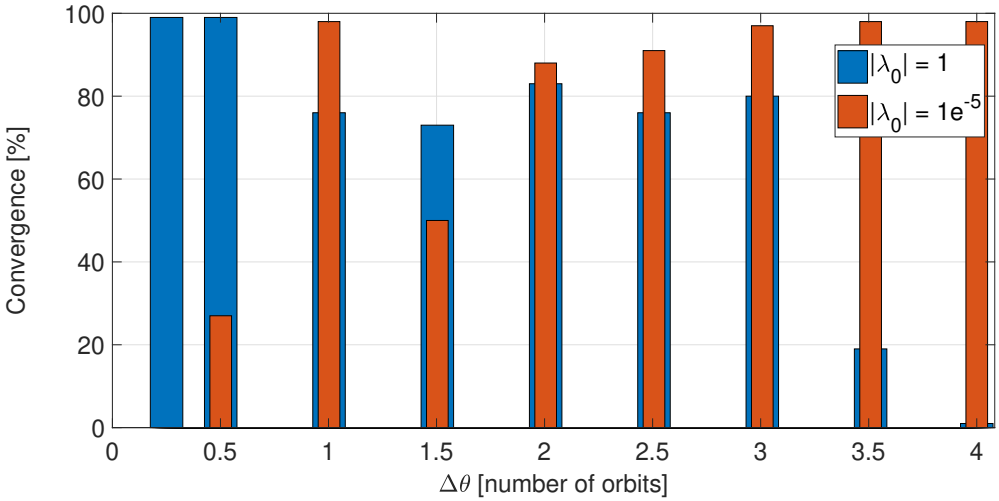

Figure 40: Convergence trend of the random search of EOP.

Δθ (number of orbits)	Convergence	
	FOP	EOP
0.1	✓	✓
3	✓	✓
3.25	✓	
3.5	✓	
4	✓	

Table 4: Convergence as function of Δθ of EOP and FOP when costates are guessed with ACT.

5

CONCLUSIONS AND FUTURE DEVELOPMENTS

In this chapter the final considerations about this work are reported, as well as the possible future developments.

5.1 CONCLUSIONS

5.1.1 *Methods*

In this work four different approaches to design a collision avoidance manoeuvre are proposed. The first one consists in the conversion of an impulsive manoeuvre to a finite-burn arc, through an indirect optimization method. The impulsive manoeuvre point is considered the middle point of the thrust arc, and the impulsive $\Delta\boldsymbol{v}$ is distributed over the arc bounded by the initial and final states, which are found by propagating backward and forward from the impulsive manoeuvre point over the pre-impulse and post-impulse trajectories. The fuel-optimal formulation of the OCP requires the use of a *continuation method* to obtain the optimal discontinuous control law: the bang-bang thrust profile is approximated with an exponential function, and the discontinuous profile is gradually achieved through an iterative procedure.

In the second approach the problem is stated as an OCP where the P_c computed with the Chan model is inserted in the cost function as terminal cost. For the FOP, the cost function is $J = P(t_f, \boldsymbol{r}_f) + \int_{t_i}^{t_f} \frac{T_{max}}{c_e} u dt$, while for the EOP it is $J = P(t_f, \boldsymbol{r}_f) + \int_{t_i}^{t_f} \boldsymbol{a}_c \boldsymbol{a}_c^T dt$, where $T_{max}, c_e, \boldsymbol{a}_c, u$ are the maximum thrust available, the effective velocity, the control acceleration and the thrust ratio $u \in [0, 1]$, respectively. Through the application of calculus of variations, FOP and EOP translate in the resolution of a TPBVP, with the BCs consisting in the initial state and final costate. The TPBVP associated to the FOP is solved with a collocation method, while EOP is solved through the adoption of the shooting method.

These processes are carried on a grid of initial manoeuvre points along the nominal orbit, and through the application of weights W in the cost function it is possible to tune the P_c for the same manoeuvre point: the weights change the ratio between the terminal and the path cost, so that a larger weight on P_c yields a lower collision probability at fuel's or energy's expense.

The analysis of the spacecraft positions at the time of closest approach, after the manoeuvres, showed the presence of different solution to the FOP/EOP minimization problem. A random search for the EOP solutions allowed us to find four solution branches, which cause discontinuities in the probability profile. In order to have solutions convergent all to the same branch, the solution found for a manoeuvre point is used as initial guess for the next $\Delta\theta$.

In the third approach the EOP is linearised, and an analytical solution is obtained by computing and manipulating the STM. The problem translates in a transfer between two fixed states: the direction of maximum change of P_c at the time of

closest approach, $\mathbf{d}_{max}$, is found through a simple eigenvalue problem. The final position of the spacecraft $\mathbf{r}_f$ is set to be along this direction, in order to obtain the maximum change of P_c with the least deviation from the nominal trajectory. Depending on the position of $\mathbf{r}_f$ along $\mathbf{d}_{max}$, different P_c are obtained.

The fourth approach starts from the linearisation of the EOP and exploits the boundary conditions of the TPBVP associated with the EOP to find a direct relation between the terminal cost in the cost function and $\mathbf{r}_f$. The application of different weights W to the terminal cost $J = WP(t_f, \mathbf{r}_f) + \int_{t_i}^{t_f} \mathbf{a}_c \mathbf{a}_c^T dt$ affects the terminal boundary conditions of the costates. Through the STM, it is possible to obtain a set of nonlinear equations to find $\mathbf{r}_f$, function of W. Once $\mathbf{r}_f$ is obtained, P_c is immediately computed trough an analytical formula. By acting on the weight W, it is possible to tune P_c for the same manoeuvre point. Then, by means of the STM, the initial costate and the optimal control law associated to the desired P_c can be retrieved.

5.1.2 *Comparisons*

The minimum-fuel formulations obviously result to be the most efficient in terms of propellant. FBC Δm, accordingly with the conversion formulation, is constant no matter the manoeuvre point where the burn-arc starts. FOP Δm diminishes with $\Delta\theta$, as well as the achieved P_c. FBC proved to be always more efficient than FOP but close to the collision, since even for high P_c, FBC mass consumption does not change. AM is clearly the less efficient, since the energy-optimal formulation and the oscillatory behaviour of the mass both contribute negatively to the propellant consumption. SAM results are consistent with the problem formulation, since it is the linearisation of EOP. Because of the small deviations from the nominal trajectory, the linearisation does not introduce visible differences between SAM and EOP, and the mass profile can reasonably be considered identical for both the formulations, with the only difference of the SAM discontinuity close to the collision.

Regarding the computational time, SAM and AM are clearly superior to the fully numerical methods. The CT of these methods increases with the distance to collision, unlike the CT of FBC and FOP, that does not depend on $\Delta\theta$ and remains approximately constant. Nevertheless, SAM/AM CT results always lower than the ones of the other numerical methods. As expected, AM is always faster than SAM, but the difference is almost negligible. FOP resulted the most inefficient. FBC has a constant CT, since a single continuation rate is valid for all manoeuvre points. EOP CT decreases with $\Delta\theta$, because of the dependency of the shooting method on the time to collision.

Convergence is a real issues for FOP, because of the high sensitivity of this method on the continuation rate. On the other hand, when a good continuation rate is found, there are no more convergence problems. EOP is very sensitive to the initial guesses because of the presence of different solutions to the optimization problem. When ACT is used to guess the solution, the algorithm does not converge for manoeuvre points located more than 2 orbits in advance with respect to the collision. FBC always converged, as well as SAM.

5.2 FUTURE DEVELOPMENTS

The main achievement of this work is represented by the ideas behind the different proposed approaches. The methods themselves are designed in the context of circular Keplerian orbits, therefore they are suitable for preliminary analysis, but further investigation has to be done about the influence of orbital perturbations on the manoeuvres. Particular attention should be paid for the methods based on the minimum-energy formulation, since the control acceleration could reach values comparable with the ones of the perturbing accelerations caused by atmospheric drag and J_2.

Regarding the design of the fully numerical methods and SAM, it would be interesting to find a way to know a-priori the threshold P_c would reach after the manoeuvre. One way to do it, could be to find a relation between the applied weights and the last useful value of P_c, right before the solution switches to no-thrust. In this way it would be possible to know that no matter the manoeuvre point, the spacecraft would reach at least the desired P_c, once the correct weight is applied.

In minimum-energy formulation there is no bound on the mass consumption, therefore a natural improvement could be to add an automatic check in the algorithm. If the mass threshold is exceeded, another manoeuvre at higher P_c but adequate mass consumption should be computed.

BIBLIOGRAPHY

[1] Dei Tos A. Diogene. "Trajectory optimization of limited control authority spacecraft in high-fidelity models". Doctoral Dissertation. Politecnico di Milano, 2016.

[2] European Space Agency. *About Space Debris*. 2018. URL: https://www.esa.int/Our_Activities/Space_Safety/Space_Debris/About_space_debris.

[3] Richards. Arthur. et al. "Spacecraft Trajectory Planning with Avoidance Constraints Using Mixed-Integer Linear Programming". In: *Journal of Guidance, Control, and Dynamics* 25.4 ().

[4] Committee on the Peaceful Uses of Outer Space various authors. *Towards long-term sustainability of space activities: overcoming the challenge of space de- bris. A report of the International interdisciplinary congress on Space debris*. 2011. URL: http://www.oosa.unvienna.org/%20pdf/limited/AC105_C1_2011_CRP14E.pdf.

[5] C. Bombardelli. "Analytical Formulation of Impulsive Collision Avoidance Dynamics". In: *Celestial Mechanics andDynamical Astronomy* 118.2 (2013), pp. 99–114.

[6] Claudio. Bombardelli and Javier. Hernando-Ayuso. "Optimal Impulsive Collision Avoidance in Low Earth Orbit". In: *Journal of Guidance, Control, and Dynamics* (2015). DOI: 10.2514/1.G000742.

[7] F. Kenneth Chan. *Spacecraft Collision Probability*. 2008.

[8] *Conjunction Summary Message Guide*. 2014. URL: ww.space-track.org/documents/CSM_Guide.pdf.

[9] Bruce A. Conway, ed. *Spacecraft Trajectory Optimization*. Cambridge University Press, 2010. ISBN: 978-0-521-51850-5.

[10] R. Domínguez-González et al. "Analysis of uncertainties of catalogued orbital data for the update of the ESA DRAMA ARES tool". In: *booktitle*. Vol. Proceedings of the 63rd International Astronautical Congress. 2012.

[11] *Space Surveillance and Tracking in ESA's SSA programme*. 7th European Conference on Space Debris (2017).

[12] L. Fox. *The Numerical Solution of Two-Point Boundary Problems*. Ed. by Oxford Press. 1957.

[13] *Operational Collision Avoidance at ESOC*. Deutscher Luft- und Raumfahrtkongress.

[14] I. Grande-Olalla et al. "Collision risk assessment and avoidance manoeuvre strategies for satellites: new tool CORAM for ESA". In: Sixth European Space Debris Conference. 1 vols. 3.

[15] A.E. Bryson Jr.and Y.C. Ho. *Applied Optimal Control*. Ed. by D.C. Hemisphere Publishing Washington. 1975.

[16] *Iridium 33/Cosmos 2251 Collision*. 2009. URL: celestrak.com.

[17] D.F. Lawden. *Optimal Trajectories for Space Navigation*. Ed. by London Butterworths. 1963.

[18] K. Lee, C. Park, and S. Park. "Near-Optimal Guidance and Control for Spacecraft Collision Avoidance Maneuvers". In: AIAA/AAS Astrodynamics Specialist Conference.

[19] James. M. Longuski, José. J. Guzmán, and John E. Prussing. *Optimal Control Problem with Aerospace Application*. Ed. by Springer Microcosm Press. 2014. ISBN: 978-1-4614-8944-3. DOI: 978-1-4614-8945-0.

[20] F. Flohrer T.and Schmitz, ed. *Current Collision Avoidance service by ESA's Space Debris Office*. 7th European Conference on Space Debris, Darmstadt, Germany. ESA Space Debris Office.

[21] A. Morselli et al. "Collision Avoidance Maneuver Design Based on Multi-objective Optimization". In: *Advances in the Astronautical Sciences*. AAS 14-148. AAS/AIAA. Santa Fe, New Mexico, USA.

[22] . P. Russell Patera and Peterson. E. Glenn. "Space Vehicle Maneuver Method to Lower Collision Risk to an Acceptable Level". In: *Journal of Guidance, Control, and Dynamics* 26.2 ().

[23] Chris L. Ranieri and Cesar A. Ocampo. "Optimization of Roundtrip, Time-Constrained, Finite Burn Trajectories via an Indirect Method". In: *Journal of Guidance, Control, and Dynamics* 28.2 ().

[24] M. Rasotto, R. Armellin, and P. Di Lizia. "Multi-step optimization strategy for fuel-optimal orbital transfer of low- thrust spacecraft M." In: *Engineering Optimization*, (2015).

[25] Jason A. Reiter and David B. Spencer. "Solutions to Rapid Collision-Avoidance Maneuvers Constrained by Mission Performance Requirements". In: *Journal of Spacecraft and Rockets* (). DOI: 10.2514/1.A33898.

[26] L.F. Shampine and J. Kierzenka. "A BVP Solver based on residual control and the MATLAB PSE". In: *ACM Trans. Math. Softw.* 27 vols. 3. 2001, pp. 299–316.

[27] G.L. Slater, S.M. Nyram, and T.W. Williams. "Collision Avoidance for Satellites in Formation Flight". In: *Journal of Guidance, Control, and Dynamics* 29.5 ().

[28] Alessandro. Zavoli. "Indirect Optimization of Bang-Bang Control Problems and Applications to Formation Flying Missions". Doctoral Dissertation. Sapienza Università di Roma.